Article

Therapeutic genetic restoration through allogeneic brain microglia replacement

https://doi.org/10.1038/s41586-025-09461-6

Received: 30 April 2024

Accepted: 28 July 2025

Published online: 06 August 2025

Check for updates

Marius Marc-Daniel Mader[1,2,3,4,5,6], Alexa Scavetti[1,2,3], Yongjin Yoo[1,2,3], Aaron Tianyue Chai[1,2,3], Takeshi Uenaka[1,2,3] & Marius Wernig[1,2,3]✉

Migration of transplanted allogeneic myeloid cells into the brain following systemic haematopoietic stem and progenitor cell transplantation (HCT) holds great promise as a therapeutic modality to correct genetic deficiencies in the brain such as lysosomal storage diseases[1–3]. However, the toxic myeloablation required for allogeneic HCT can cause serious, life-threatening side effects, limiting its applicability. Moreover, transplanted allogeneic myeloid cells are highly vulnerable to rejection even in an immune-privileged organ like the brain. Here we report a brain-restricted, high-efficiency microglia replacement approach without myeloablative preconditioning. Contrary to previous assumptions, we found that haematopoietic stem cells are not required to repopulate the myeloid compartment of the brain environment, and Sca1$^-$ committed progenitor cells were highly efficient in replacing microglia following intracerebral injection. This finding enabled the development of brain-restricted preconditioning and avoided long-term peripheral engraftment, thus eliminating complications such as graft-versus-host disease. Evaluating its therapeutic potential, we found that our allogeneic microglia replacement method rescued the mouse model of Sandhoff disease, a lysosomal storage disease caused by hexosaminidase B deficiency. In support of the translational relevance of this approach, we discovered that human embryonic stem cell-derived myeloid progenitor cells display a similar engraftment potential following brain-restricted conditioning. Our results overcome current limitations of conventional HCT and may pave the way for the development of allogeneic microglial cell therapies for the brain.

Microglia are the main tissue-resident myeloid cells of the central nervous system (CNS) and are developmentally derived from primitive erythro-myeloid progenitors of the yolk sac[4]. Despite having a similar origin, microglia are phenotypically and transcriptionally distinct from other CNS-associated macrophage populations, which are primarily located at the CNS borders[5,6]. Microglia are dependent on colony-stimulating factor 1 receptor (CSF1R) signalling, and loss or inhibition of this receptor leads to depletion of endogenous microglia[7,8]. Normally, the CNS parenchymal myeloid niche is repopulated by residual naive microglia[9]. This emptied niche can alternatively be repopulated by haematopoietic cells with a genetic advantage in CSF1R signalling, which consequently differentiate into myeloid cells with a microglia-like phenotype[10–12]. However, under physiological conditions and without genetic engineering of donor cells, the contribution of peripheral, bone marrow-derived cells to the microglia pool is minimal in mice[13]. By contrast, parenchymal CNS engraftment of haematopoietic cells is enabled by cytotoxic measures, such as the alkylating chemotherapy or ionizing radiation used in HCT[2,3,6,14–23]. Whereas these regimens commonly lead to slow and variable engraftment, we and others have found that the combination of myeloablative preconditioning and pharmacological CSF1R inhibition results in rapid and near-complete replacement of microglia with injected bone marrow cells[3,19–21,23,24].

Systemic HCT has been identified as a gene therapy modality to treat different neurometabolic disorders, such as leukodystrophies and lysosomal storage diseases, in humans[25–28]. Preclinical data support the hypothesis that treatment effects are based on the CNS engraftment and myeloid differentiation of donor cells, thereby circumventing the blood–brain barrier and permitting direct intracerebral delivery of the missing gene product[1,2]. It therefore seems desirable to increase and accelerate the engraftment of donor cells in the CNS, given that clinical improvement based on HCT alone is still limited[29,30]. Motivated by this need, we have previously applied high-efficiency replacement of endogenous microglia, which was based on busulfan-conditioned systemic HCT of syngeneic wild-type cells, in a lysosomal storage disease mouse model with therapeutic benefit[3]. Notably, myeloid replacement in the CNS seems to also hold therapeutic implications for other neurological disorders, such as neurodegenerative and neuroinflammatory diseases[23,24,31,32].

Thus far, however, efficient microglia replacement requires cytotoxic conditioning regimens with body-wide side effects, limiting its

[1]Institute for Stem Cell Biology and Regenerative Medicine, Stanford University School of Medicine, Stanford, CA, USA. [2]Department of Pathology, Stanford University School of Medicine, Stanford, CA, USA. [3]Department of Chemical and Systems Biology, Stanford University School of Medicine, Stanford, CA, USA. [4]Present address: Department of Neurosurgery, University Medical Center Hamburg-Eppendorf, Hamburg, Germany. [5]Present address: Department of Pediatric Hematology and Oncology, University Medical Center Hamburg-Eppendorf, Hamburg, Germany. [6]Present address: Research Institute Children's Cancer Center, Hamburg, Germany. ✉e-mail: wernig@stanford.edu

applicability to chronic diseases[3,19–21,23,24]. Moreover, certain conditions may benefit from brain-restricted myeloid engraftment without replacement of the entire haematopoietic system. Attempts to deliver haematopoietic donor cells without genetic advantage directly into the brain yielded only localized, slow or inefficient engraftment[3,18,20]. High-efficiency microglia replacement has also not been achieved in allogeneic transplantation settings. To overcome these limitations, here we sought to develop an allogeneic brain-restricted therapeutic microglia replacement strategy without the need for genetic engineering of donors or recipients and without systemic cytotoxic preconditioning.

Replacing microglia with reduced myelotoxicity

On the basis of our previous findings that ex vivo expanded mouse haematopoietic stem and progenitor cells (HSPCs; derived from primary lineage (Lin)$^-$Kit$^+$Sca1$^+$CD150$^+$CD48$^-$ cells) can repopulate the CNS myeloid niche with high efficiency in the context of systemic busulfan-induced myeloablative transplantation in combination with CSF1R inhibition with a PLX5622-containing diet (M.M.-D.M. et al., unpublished data), here we evaluated the effect of different preconditioning elements on the efficiency of microglia replacement following direct intracerebroventricular (ICV) injection of HSPCs (Extended Data Fig. 1a). Two weeks after cell injection, we observed no relevant engraftment in non-preconditioned transplantations and only a slight increase if the transplantation was preceded by either myeloablation with busulfan or a PLX5622-containing diet (Extended Data Fig. 1b,c). Combined busulfan and PLX5622 preconditioning visibly enhanced the transplantation efficacy, albeit with apparent variability. ICV injection of HSPCs also led to undesired systemic engraftment of HSPC-derived cells in the myeloablative experimental groups (Extended Data Fig. 1c).

Our next goal was to improve brain conditioning before transplantation. First, we evaluated whether parenteral application of CSF1R inhibitors allows more rapid depletion of naive microglia (Extended Data Fig. 1d–f). We found that 3–4 daily intraperitoneal (i.p.) injections of either PLX5622 or PLX3397 markedly reduced the number of naive microglia in the brain. We then reasoned that microglia should selectively become more sensitive to busulfan as they proliferate and regenerate lost cells after CSF1R inhibition[9]. Therefore, we injected mice with PLX3397 a day before a 2-day busulfan treatment followed by another round of PLX3397 injections, after which mice were transplanted with green fluorescent protein (GFP)-expressing HSPCs by ICV injection (Extended Data Fig. 1g). We also tested the effect of omitting or extending the busulfan treatment. Recipient mice also received systemic injections of Kusabira Orange (KUO)-labelled whole-bone marrow cells subsequent to ICV transplantation to rescue potential myeloablative toxicity. The 4-day busulfan regimen led to high early mortality, whereas the survival of mice undergoing the 2-day regimen was not reduced. As before, CSF1R inhibition alone did not permit relevant cell engraftment in the brain, whereas the combination with the 2-day busulfan regimen enabled robust graft chimerism at a level of approximately 35–90% after 2 weeks (Extended Data Fig. 1h,i). Peripherally injected KUO$^+$ rescue whole-bone marrow cells did not contribute to graft chimerism in the brain. Notably, although the 2-day dose of busulfan reduced the fraction of Kit$^+$Sca1$^+$Lin$^-$ (KSL) cells in the bone marrow, it did not lead to complete myeloablation. Again, we detected donor-derived cells in the blood circulation (up to ~25%) and moreover identified up to around 10% donor-derived KSL cells in the femur bone marrow. Unexpectedly, we found that i.p. injections of PLX5622 in a comparable regimen did not result in brain engraftment of donor cells (Extended Data Fig. 1j,k).

Next, we explored whether head-restricted irradiation would be comparable to busulfan injections to further reduce systemic toxicity (Fig. 1a). Indeed, replacing 2-day busulfan treatment with head-restricted irradiation on 1 day, we consistently observed over 90% microglia replacement as measured by flow cytometry when irradiation was combined with PLX3397 (Fig. 1b). Histologically, we confirmed a brain-wide distribution with some variability in the density of grafted cells in circumscribed areas (Fig. 1c and Extended Data Fig. 1l,m). Engrafted donor cells exhibited a ramified morphology and expressed the myeloid marker IBA1 (Fig. 1d and Extended Data Fig. 1m). Combining PLX5622 with irradiation also resulted in robust donor-derived brain chimerism, but the level of chimerism was considerably lower than with PLX3397 (Fig. 1b).

As expected, none of the experimental regimens led to systemic myeloablation, as confirmed by the persisting presence of KSL cells in the femur bone marrow (Fig. 1b). Although donor-derived cells were present at low levels in the peripheral blood, no integration was detected in the KSL population of the peripheral bone marrow in this first cohort. In an independent cohort, we confirmed high-level (>80%) brain engraftment of donor-derived cells but observed a higher level of graft-derived chimerism in the peripheral blood as well as in the KSL population of the bone marrow (Extended Data Fig. 1n,o). A reduced irradiation dose (50% reduction) was still sufficient to generate a median donor-derived chimerism level of 57.7%. Finally, we confirmed the long-term presence of donor cells in the brain (median chimerism of 85.3% after ~8 months; Extended Data Fig. 1p).

In contrast to naive microglia, the expression of microglial homeostatic markers was low (TMEM119) to absent (P2RY12) in transplanted cells (Extended Data Fig. 2).

In summary, direct transplantation of HSPCs into the CNS following brain-restricted conditioning can lead to robust and high-level replacement of brain microglia. In all conditions, we still saw some level of contribution to peripheral blood and therefore had not accomplished brain-restricted incorporation.

CNS myeloid repopulation does not require HSCs

To develop a truly brain-specific microglia replacement approach, we further dissected the contribution of haematopoietic subpopulations to microglia repopulation[33]. We had previously demonstrated that systemic transplantation of haematopoietic stem cells (HSCs) results in a higher CNS engraftment efficiency than transplantation of more restricted haematopoietic progenitor cells (HPCs) or various monocyte populations[3]. However, it remained unclear whether this was based on a greater CNS engraftment potential of HSCs or solely superior proliferation in the periphery. Here we took advantage of our previous finding that primary astrocytes strongly induce myeloid differentiation of HSPCs (M.M.-D.M. et al., unpublished data) (Fig. 2a,b and Extended Data Fig. 3a,b). Unexpectedly, both immunophenotypic long-term and short-term HSCs (Lin$^-$CD127$^-$Kit$^+$Sca1$^+$CD34$^-$CD150$^+$ and Lin$^-$CD127$^-$Kit$^+$Sca1$^+$CD34$^-$CD150$^-$, respectively) isolated from bone marrow led to no or nearly no myeloid generation and were outcompeted by repopulating naive microglia. As expected, immunophenotypic common lymphoid progenitors (CLPs) also did not produce any myeloid progeny. By contrast, immunophenotypic common myeloid and granulocyte-monocyte progenitors (CMPs and GMPs, respectively) demonstrated the strongest repopulation potential, notably surpassing Ly6C^{high} monocytes, which have previously been reported to infiltrate and repopulate the CNS myeloid niche[16,34]. We then validated these findings in the context of ex vivo propagated haematopoietic graft cells, using a competitive setting in which bulk HSPCs were co-plated with defined subpopulations (Fig. 2c and Extended Data Fig. 3c,d). Again, immunophenotypic CMPs and especially GMPs showed the strongest myeloid repopulation potential, whereas HSCs (Lin$^-$CD127$^-$Kit$^+$Sca1$^+$CD150$^+$ or Lin$^-$CD127$^-$Kit$^+$Sca1$^+$CD150$^-$) performed poorly. We further validated these findings by direct competition of KSL cells, which include HSCs and multipotent progenitors, with Kit$^+$Sca1$^-$Lin$^-$ (KL) myeloid progenitors (HPCs) (Fig. 2d and Extended Data Fig. 3c,e). We found that Sca1 expression was indeed associated with reduced competitiveness for myeloid repopulation.

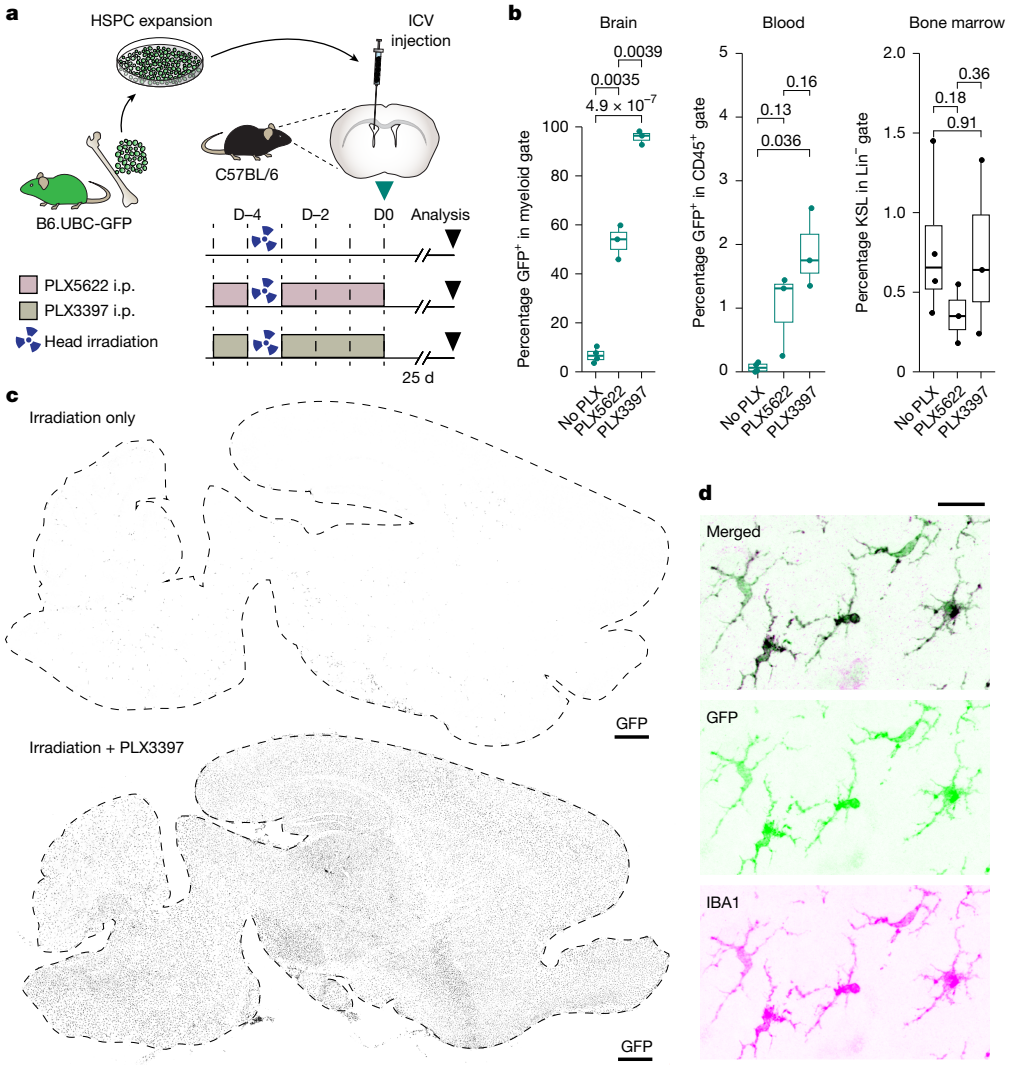


Fig. 1 | A high-efficiency non-myeloablative microglia replacement approach. **a**, Experimental design. B6.UBC-GFP HSPCs (200×10^3) were transplanted into recipient mice (C57BL/6, both sexes; $n = 3$–4 mice per group). Periprocedural mortality occurred in one PLX3397-treated mouse. D, day. **b**, Flow cytometry quantification (contralateral brain hemisphere). $n = 4$, 3 and 3 mice per group, respectively (from left to right). Statistical analysis was performed by two-sided Welch's *t* test. No GFP$^+$ cells were detected in the KSL population of the femur bone marrow in any experimental group. Box plot elements represent the median (centre line), first and third quartiles (lower and upper hinges), and lowest and highest values within 1.5 times the interquartile range (IQR) from the hinge (whiskers). **c**, Sagittal brain sections of the ipsilateral hemisphere with immunofluorescence staining for GFP. The dashed lines depict the CNS border. Scale bars, 200 µm. **d**, Cortical brain myeloid cells. Immunofluorescence staining was evaluated in $n = 3$ ipsilateral hemispheres of mice treated with irradiation + PLX3397, confirming similar morphology and protein expression patterns. Scale bar, 20 µm.

These findings suggested that Sca1$^-$ HPCs may be highly competent to replace endogenous microglia in vivo, although they are unable to give rise to long-lasting haematopoietic engraftment in bone marrow and peripheral blood. Indeed, unlike Sca1$^+$ HSPCs, ICV-injected Sca1$^-$ HPCs efficiently repopulated the brain of preconditioned mice and showed poor or no engraftment in peripheral blood and bone marrow (Fig. 2e,f). Notably, Sca1-depleted cells had a much higher capacity to repopulate the brain than Sca1-enriched cells when placed in direct competition (Fig. 2g).

Allogeneic myeloid cell engraftment in the CNS

High-efficiency microglia replacement strategies in mice have thus far been limited largely to syngeneic/autologous transplantation[2,3,14,16–21,23,24]. However, without genetic engineering, autologous transplantation would not be therapeutic for genetic diseases. Because the brain is an immune-privileged site, we attempted allogeneic microglia replacement, transplanting B6.UBC-GFP (C57BL/6 background) cells into B6/129S mixed-background mice (Fig. 3a). Despite our high-efficacy intracerebral HSPC transplantation approach, donor cells were rejected in most recipient mice within a few weeks of transplantation (Fig. 3b,c). Graft rejection was consistently accompanied by T cell infiltration of the brain, which was also present in transplantations within the B6/129S strain but was not observed in syngeneic transplantations (Fig. 3d,e). We then evaluated two main strategies to prevent graft rejection. We combined transplantation of Sca1$^-$ HPCs with either a co-stimulation blockade regimen[35] or cyclophosphamide-based tolerance induction[36], for which we primed the immune system with HSPCs, whole-bone marrow cells and/or splenocytes (Fig. 3f). Splenocyte-only priming resulted in high mortality, whereas the other regimens were better tolerated (Fig. 3f) and prevented graft rejection at 4 weeks after transplantation (Fig. 3g). Co-stimulation blockade effectively prevented T cell infiltration into the brain. By contrast, we observed elevated T cell levels especially with the HSPC priming regimen, indicative of a developing graft rejection reaction. As the only regimen,

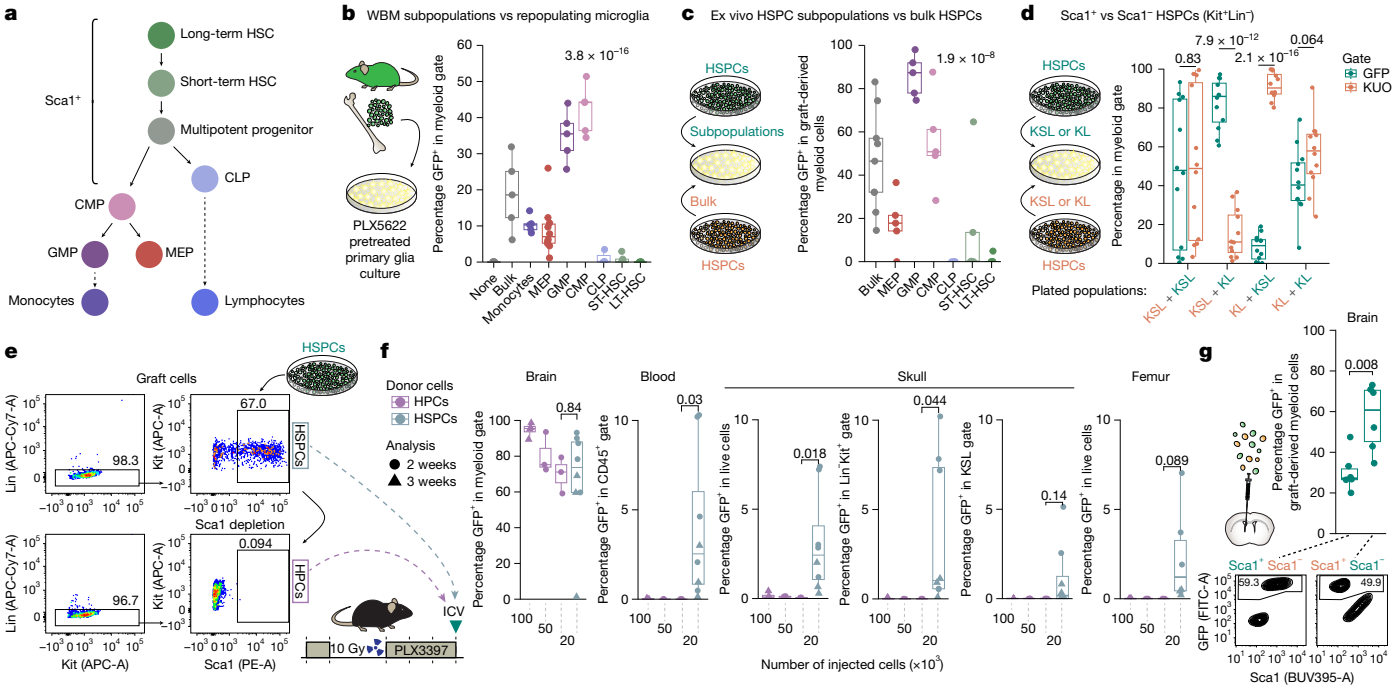


Fig. 2 | HSCs are not required for CNS myeloid niche repopulation. **a**, Haematopoietic developmental hierarchy[33]. MEP, myelo-erythroid progenitor. **b**, Whole-bone marrow (WBM) subpopulations or bulk whole-bone marrow cells (100 cells per 1.9 cm^2) from B6.UBC-GFP mice were plated on PLX5622-pretreated primary C57BL/6 glia. Flow cytometry was performed after 10 days. $n = 5, 5, 5, 10, 5, 5, 3, 5$ and 5 culture wells per condition, respectively (from left to right). Statistical analysis was performed by one-way analysis of variance (ANOVA). ST, short term; LT, long term. **c**, HSPC subpopulations (B6.UBC-GFP) were plated together with bulk HSPCs (B6.KUO) on PLX5622-pretreated primary C57BL/6 glia (100 cells each per 1.9 cm^2). Flow cytometry was performed after 13 days. $n = 9, 5, 5, 5, 5, 5$ and 5 culture wells per condition, respectively (from left to right). Statistical analysis was performed by one-way ANOVA. **d**, KSL (Kit$^+$Sca1$^+$Lin$^-$) or KL (Kit$^+$Sca1$^-$Lin$^-$) cells derived from either B6.UBC-GFP or B6.KUO HSPCs were plated on CSF1R-knockout glia (2 × 100 cells per 1.9 cm^2) in serum-free conditions. Flow cytometry was performed after 20 days. $n = 12$ culture wells per condition. Statistical analysis was performed by two-sided Welch's t test. **e**, Representative flow cytometry evaluation of graft cells (B6.UBC-GFP) before ICV transplantation. HPCs were generated by MACS depletion of HSPCs and transplanted into preconditioned recipient mice (C57BL/6, both sexes). Mice were transplanted with 20×10^3 ($n = 3$ mice), 50×10^3 ($n = 3$ mice) or 100×10^3 ($n = 4$ mice) HPCs. The HSPC control group received 20×10^3 cells ($n = 8$ mice). **f**, Flow cytometry quantification of donor-derived engraftment in different compartments (2 and 3 weeks after transplantation). $n = 10$ mice in the HPC group and 8 mice in the HSPC group (femur bone marrow analysed for $n = 6$ mice in the HSPC group). Statistical analysis was performed by two-sided Welch's t test. **g**, Mixed HSPCs were ICV transplanted (either GFP$^+$ Sca1-enriched with KUO$^+$ Sca1-depleted cells or KUO$^+$ Sca1-enriched with GFP$^+$ Sca1-depleted cells). Flow cytometry plots show the live-cell gate of transplanted cells. Brain analysis was performed 3 weeks after transplantation. Graft-derived myeloid cells were defined as GFP$^+$/KUO$^+$CD45$^+$ CD11b$^+$ cells. $n = 6$ mice per group. Statistical analysis was performed by two-sided Welch's t test. Box plot elements represent the median (centre line), first and third quartiles (lower and upper hinges), and lowest and highest values within 1.5 times the IQR from the hinge (whiskers).

priming transplantation with whole-bone marrow cells (combined with splenocytes), which was timed to take place after head irradiation, led to a substantial level of peripheral blood donor chimerism (Fig. 3h). Moreover, we evaluated the peripheral blood for signs of immune activation indicative of active or impending graft rejection (Fig. 3h and Extended Data Fig. 4), which was present in the form of an increase in the effector memory T cell fraction for both CD4$^+$ and CD8$^+$ T cells, as well as an increase in the number of regulatory T cells. These changes were absent with co-stimulation blockade (specifically for CD4$^+$ T cells) but were observable in the cyclophosphamide-based regimens. Thus, co-stimulation blockade was the simplest, most effective intervention to prevent rejection of transplanted brain myeloid cells for at least 4 weeks. Notably, the same co-stimulation blockade regimen with booster injections every 2 weeks allowed graft survival for up to 9 months after transplantation, albeit with a lower and more variable level of chimerism (Fig. 3i). Finally, we confirmed the applicability of this approach in an HLA-mismatched transplantation setting by transplanting B6.UBC-GFP cells into FVB mice (Fig. 3j).

Microglia replacement rescues *Hexb* deficiency

Next, we set out to evaluate the potential of allogeneic microglia replacement to restore disease gene expression in a mouse model of Sandhoff disease, a hereditary neurodegenerative lysosomal storage disorder[37]. Homozygous knockout of the *Hexb* gene leads to deficiency of the β-hexosaminidase isoenzymes with consequent accumulation of G_{M2} ganglioside and other glycolipids and oligosaccharides in lysosomes in the brain. Affected mice present with progredient neurological deficits and have a markedly reduced life expectancy. Notably, *Hexb* is a gene strongly expressed in microglia, which encouraged us to explore whether allogeneic microglia replacement with wild-type cells would translate into a therapeutic benefit. To this end, we performed ICV transplantation of B6.UBC-GFP HPCs into *Hexb*$^{-/-}$ recipient mice (B6/129S) with peri-transplantation co-stimulation blockade at an age of around 6 weeks (cell therapy (CT) group; Fig. 4a). Histological assessment at approximately 12 weeks after transplantation confirmed the persistence of transplanted GFP$^+$ cells in the majority of grafted mice, albeit to a varying extent, presumably owing to delayed immune rejection (Extended Data Fig. 5a,b). Crucially, and as expected, we detected no signs of graft-versus-host disease (Extended Data Fig. 5c).

Notably, the presence of *Hexb*$^{+/+}$ grafted myeloid cells resulted in partially rescued β-hexosaminidase activity, which was most prominent not only directly in grafted cells but also in adjacent neuron-specific anatomical areas, for example, in the dentate gyrus, hippocampal subfields and cortex (Fig. 4b and Extended Data Fig. 5d,e). *Hexb*$^{-/-}$ mice had

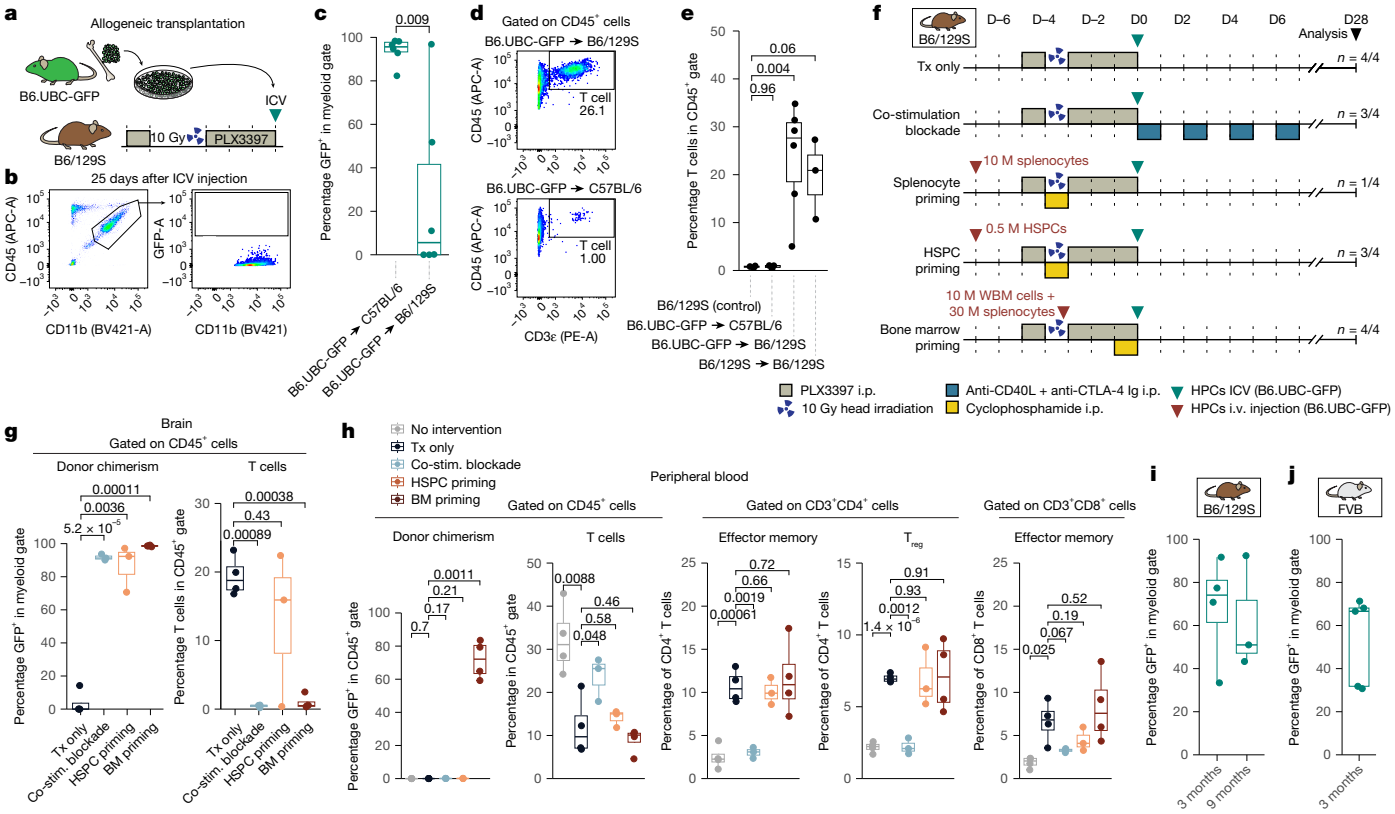


Fig. 3 | Co-stimulation blockade enables allogeneic myeloid cell engraftment in the CNS. a, HSPCs (200×10^3 per mouse) from B6.UBC-GFP donor mice were ICV transplanted in preconditioned B6/129S mixed-background recipients. **b**, Representative flow cytometry plots for brain myeloid cell analysis. **c**, Quantification of donor-derived GFP$^+$ chimerism in brain myeloid cells by flow cytometry. $n = 6$ mice per group. C57BL/6 host mice represent the animals shown in Fig. 1b and Extended Data Fig. 1o. Statistical analysis was performed by two-sided Welch's t test. **d**, Representative flow cytometry plots for brain T cell quantification. **e**, Quantification of T cell representation in the brain by flow cytometry. $n = 6$ mice in the B6.UBC-GFP → B6/129S group and $n = 3$ mice in the other groups. Statistical analysis was performed by two-sided Welch's t test. **f**, Experimental design to evaluate regimens of immune modulation to enable allogeneic microglia replacement (B6.UBC-GFP into B6/129S, both sexes). A total of 100×10^3 Sca1$^-$ HPCs were transplanted per mouse. Numbers (n) represent mice that survived until the 4-week endpoint out of the total transplanted replicates. Ig, immunoglobulin; i.v., intravenous; M, million; Tx, transplantation. **g**, Flow cytometry quantification of GFP$^+$ donor chimerism and T cell fraction in the brain (in the hemisphere contralateral to ICV injection). $n = 4, 3, 3$ and 4 mice per group, respectively (from left to right). Statistical analysis was performed by two-sided Welch's t test. Co-stim., co-stimulation. **h**, Flow cytometry characterization of the peripheral blood. The 'no intervention' group consisted of littermates without transplantation or other interventions. $n = 4, 4, 3, 3$ and 4 mice per group, respectively (from left to right). Statistical analysis was performed by two-sided Welch's t test. T_{reg}, regulatory T cell. **i**, Flow cytometry quantification of myeloid donor-derived chimerism 3 ($n = 4$ mice) and 9 ($n = 3$ mice) months after allogeneic ICV transplantation of B6.UBC-GFP HPCs into B6/129S host mice of either sex using the co-stimulation blockade regimen with additional booster injections every 2 weeks. **j**, Flow cytometry quantification of myeloid donor-derived chimerism 3 months after allogeneic ICV transplantation of B6.UBC-GFP HPCs into FVB host mice using the co-stimulation blockade regimen with additional booster injections every 2 weeks. $n = 5$ mice. Statistical analysis was performed by two-sided Mann–Whitney U test comparing 3-month chimerism with that in B6/129S hosts: $P = 0.19$. Box plot elements represent the median (centre line), first and third quartiles (lower and upper hinges), and lowest and highest values within 1.5 times the IQR from the hinge (whiskers).

reduced locomotor activity and impaired explorative behaviour in an open-field set-up, which we found rescued in the CT group (Fig. 4c,d and Extended Data Fig. 5f). Neurological examinations and the rotarod behaviour test demonstrated progressive deficits in motor function and coordination in *Hexb*$^{-/-}$ mice, beginning at week 10 (Fig. 4e,f). Notably, transplantation of *Hexb*$^{+/+}$ donor cells clearly ameliorated this presentation, whereas mock treatment, in which transplanted cells were derived from *Hexb*$^{-/-}$ donors, did not result in a significant therapeutic effect. Transplanted mice in which histologically more than half of the brain was engrafted with GFP$^+$ cells demonstrated fewer motor deficits at 17 weeks (neuro score of ≤4; time of >100 s on the rotarod), whereas there was pronounced variability in mice with lower levels of donor chimerism (Fig. 4g and Extended Data Fig. 5g).

Untreated *Hexb*$^{-/-}$ mice in our study had a median survival age of 135 days, with no mouse surviving longer than 155 days (Fig. 4h). At around 18 weeks of age (the a priori endpoint for histological assessment), the rate of mortality due to neurological deterioration was reduced in the CT group (10.5%; 2/19) compared with mock-treated mice (50.0%; 5/10; two-sided Fisher's exact test, $P = 0.03$). Notably, on necropsy, no GFP$^+$ cells were detected in the brains of the two CT mice who died early (Extended Data Fig. 5h). We followed five mice from the CT group past 18 weeks of age and observed only one mortality event in this subgroup up to the end of follow-up at the age of around 35 weeks (250 days). Even though these long-term survivor mice developed hindlimb paralysis over time (Extended Data Fig. 5i), they maintained basic ambulatory ability (Extended Data Fig. 5j). Thus, the allogeneic cell therapy caused a pronounced survival benefit compared with both control groups (Fig. 4h).

We further corroborated the therapeutic effect in the CT group through histological evaluation of pathological glycolipid accumulation in the hippocampus by periodic acid-Schiff (PAS) stain at around 18 weeks of age (Fig. 4i,j). In line with previous reports, we observed pathological storage of PAS$^+$ material in *Hexb*$^{-/-}$ mice, particularly prominent in the CA3 region[37]. However, this was robustly prevented

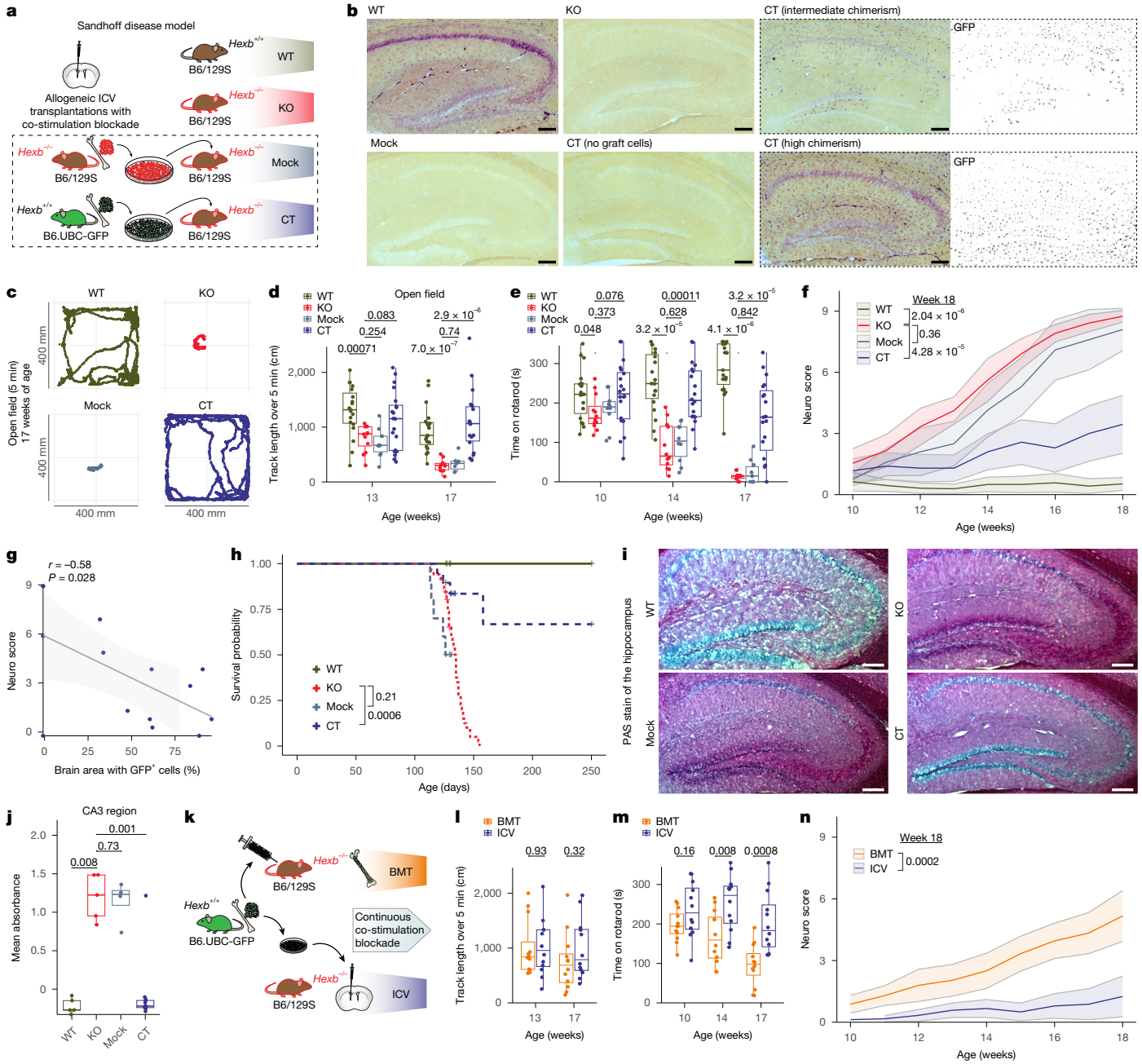


Fig. 4 | Genetic rescue of *Hexb* deficiency through allogeneic microglia replacement. a, Allogeneic ICV transplantation (100×10^3 Sca1$^-$ HPCs) in mice of both sexes at around 6 weeks of age. WT, wild type; KO, knockout. **b**, Representative images of in situ β-hexosaminidase determination and GFP immunofluorescence in the hippocampus. Twenty-seven mice were evaluated. Scale bars, 200 µm. **c**, Representative open-field traces over 5 min in approximately 17-week-old mice. **d**, Open-field test. $n = 61$ mice in total (WT, $n = 19$; KO, $n = 12$; mock, $n = 10$; CT, $n = 20$). Statistical analysis was performed by two-sided Mann–Whitney *U* test. **e**, Rotarod test. $n = 61$ mice in total (WT, $n = 19$; KO, $n = 12$; mock, $n = 10$; CT, $n = 20$). Statistical analysis was performed by two-sided Mann–Whitney *U* test. **f**, Neuro score. $n = 61$ mice in total (WT, $n = 19$; KO, $n = 12$; mock, $n = 10$; CT, $n = 20$). Lines represent the mean with the 95% confidence interval (CI). Statistical analysis was performed by two-sided Mann–Whitney *U* test. **g**, Correlation analysis. $n = 14$ mice in the CT group. The regression line is based on a linear model (the shaded area is the CI); *r* is Pearson's correlation coefficient. Statistical analysis was performed by two-sided test. **h**, Survival analysis. $n = 103$ mice in total (WT, $n = 22$; KO, $n = 51$; mock, $n = 10$; CT, $n = 19$). Thirty-six mice were censored at around 18 weeks for tissue collection (WT, $n = 11$; KO, $n = 8$; mock, $n = 5$; CT, $n = 11$). Five mice in the CT group were followed beyond 18 weeks until they reached an age of 250 days (4 of 5 survived). *P* values are based on a Cox proportional-hazards regression model for KO, mock and CT (with the exact partial likelihood method to handle ties). **i**, Representative PAS staining of the hippocampus at around 18 weeks of age. Scale bars, 200 µm. Twenty-six mice were evaluated. **j**, Quantification of the mean absorbance in the unmixed magenta channel in the CA3 region. $n = 5, 5, 4$ and 12 mice per group, respectively (from left to right). Statistical analysis was performed by two-sided Mann–Whitney *U* test. **k**, *Hexb*$^{-/-}$ mice of both sexes received either allogeneic bone marrow transplantation (BMT) or allogeneic ICV transplantation of wild-type GFP$^+$ donor cells at around 6 weeks of age (with booster injections of co-stimulation blockade). **l**, Open-field test. $n = 12$ mice per group. Statistical analysis was performed by two-sided Mann–Whitney *U* test. **m**, Rotarod test. $n = 12$ mice per group. Statistical analysis was performed by two-sided Mann–Whitney *U* test. **n**, Neuro score. $n = 12$ mice per group. Lines represent the mean with 95% CI. Statistical analysis was performed by two-sided Mann–Whitney *U* test. Box plot elements represent the median (centre line), first and third quartiles (lower and upper hinges), and lowest and highest values within 1.5 times the IQR from the hinge (whiskers).

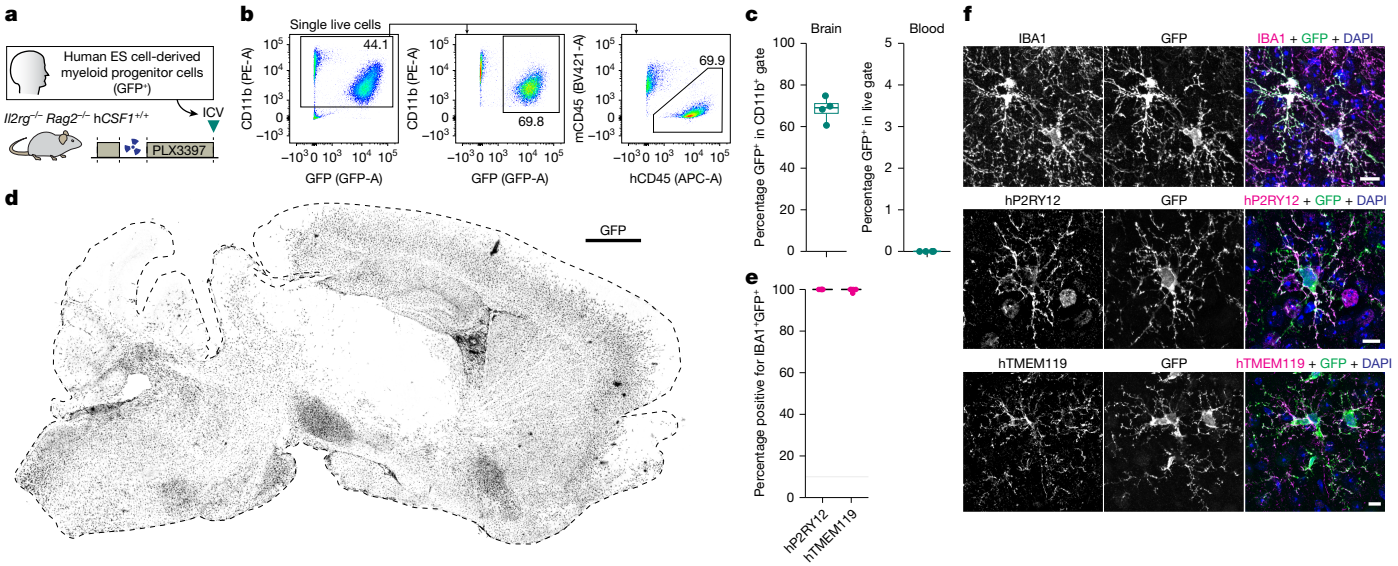


Fig. 5 | Replacement of microglia with human induced myeloid progenitor cells. a, GFP-labelled human ES cells were induced to generate myeloid progenitor cells, which were transplanted into adult preconditioned *Il2rg*$^{-/-}$*Rag2*$^{-/-}$h*CSF1*$^{+/+}$ mice of either sex through bilateral ICV injection (500×10^3 cells per recipient in total). Preconditioning consisted of 2 days of PLX3397, head-restricted irradiation with 11 Gy and another 7 days of PLX3397. **b**, Representative flow cytometry gating of brain tissue demonstrating GFP and human CD45 (hCD45) expression in graft-derived cells versus mouse CD45 (mCD45) expression in endogenous cells. **c**, Flow cytometry quantification of graft-derived chimerism in the brain and peripheral blood around 3 weeks after transplantation ($n = 4$ mice). **d**, Immunofluorescence staining for GFP. The dashed line schematically indicates the brain border. Four mice were evaluated with comparable findings. Scale bar, 100 µm. **e**, Quantification of immunofluorescence colocalization of human P2RY12 ($n = 262$ cells) and human TMEM119 ($n = 257$ cells) with IBA1$^+$GFP$^+$ cells in the brain 60 days after transplantation. $n = 5$ mice per stain. **f**, Representative immunofluorescence staining for IBA1, human P2RY12 and human TMEM119 at 60 days after transplantation. Evaluated in five mice with comparable findings. Scale bars, 10 µm. Box plot elements represent the median (centre line), first and third quartiles (lower and upper hinges), and lowest and highest values within 1.5 times the IQR from the hinge (whiskers).

in almost all *Hexb*$^{-/-}$ mice transplanted with *Hexb*$^{+/+}$ donor cells—despite the varying levels of remaining donor cells in individual animals at the time of analysis. This can be explained by previous enzyme substitution through grafted and then rejected cells, leading to a delayed onset of pathological changes and slower disease progression, which is in line with our clinical findings (Fig. 4g and Extended Data Fig. 5g).

Syngeneic bone marrow transplantation has previously been reported to slow neurological deterioration in a mouse model of Sandhoff disease[38]. To further evaluate the therapeutic effect of our brain-specific microglia replacement approach, we directly compared it to allogeneic bone marrow transplantation of wild-type cells using co-stimulation blockade (Fig. 4k). As a prerequisite, we ensured that allogeneic bone marrow transplantation together with co-stimulation blockade resulted in a level of donor chimerism comparable to that in syngeneic bone marrow transplantation (Extended Data Fig. 5k). No major graft-versus-host reaction was detectable in mice with allogeneic transplantation (Extended Data Fig. 5l). Although bone marrow transplantation with wild-type cells ameliorated neurological deficits in *Hexb*$^{-/-}$ mice (compare the mice in Fig. 4l–n to the untreated mice in Fig. 4d–f), we observed significant additional improvement with our ICV transplantation approach, especially with respect to motor function and coordination.

In summary, our histological and behavioural data demonstrate that genetic correction through allogeneic microglia replacement can counteract endogenous enzyme deficiency, improve neurological deficits, prolong survival and reduce neuropathological changes in a mouse model of Sandhoff disease.

Microglia replacement with human myeloid progenitors

Finally, we aimed to evaluate whether our microglia transplantation method can be applied to human cells. We generated human embryonic stem (ES) cell-derived myeloid progenitor cells in vitro and transplanted them into immunocompromised *Il2rg*$^{-/-}$*Rag2*$^{-/-}$ mice that carried humanized *CSF1* alleles and were preconditioned with head irradiation and PLX3397 (Fig. 5a). We observed robust engraftment of CD45$^+$CD11b$^+$ human cells at a level of around 70% (Fig. 5b–d). Engrafted cells exhibited a complex ramified morphology and expressed the common myeloid marker IBA1, as well as P2RY12 and TMEM119, markers characteristic of homeostatic microglia (Fig. 5e,f). These results show that our optimized myeloid niche preconditioning allows engraftment of human ES cell-derived myeloid progenitor cells into the adult brain without the need for genetic engineering of donor cells.

Discussion

Here we describe a strategy for the replacement of endogenous microglia with intracranially delivered haematopoietic cells that is not reliant on systemic HCT and myeloablation. In line with previous studies of systemic transplantation[3,19–21,23,24], we found that fast and highly efficient repopulation of the CNS myeloid niche is dependent on the combination of transient CSF1R-mediated microglia depletion with a cytotoxic treatment, which can be either a chemotherapeutic agent or ionizing radiation. By short-term inhibition of the CSF1R of naive microglia before cytotoxic conditioning and subsequent additional CSF1R inhibition, we were able to increase replacement efficiency, reduce systemic toxicity and shorten the overall length of the experimental protocol.

We observed an unexpected discrepancy, with the resulting donor-derived brain chimerism depending on the specific CSF1R inhibitor drug used; pretreatment with PLX3397 consistently led to more efficient graft repopulation than pretreatment with PLX5622. Both molecules are strong inhibitors of CSF1R[39]. However, a main difference between the two drugs is the high specificity of PLX5622 for CSF1R, whereas PLX3397 exhibits more off-target effects on related tyrosine kinase receptors, including Kit and FLT3 (ref. 39). Despite these

molecules having similar half-maximal inhibitory concentrations in vitro[39], PLX5622 has commonly required higher concentrations than PLX3397 to achieve efficient microglia depletion[39–41]. It is possible that co-inhibition of non-CSF1R receptor tyrosine kinases reduces the regeneration capacity of the few remaining CSF1R inhibitor-resistant microglial cells. The effect of PLX3397 on haematopoiesis and the peripheral haematopoietic system has been controversial. Although one study reported a cellular reduction in the myeloid compartment of the bone marrow[42], this was not replicated in a second study[43], and a third study showed even an increase in HSCs and myeloid progenitors without significant changes in blood myeloid populations[41]. Anti-CSF1R effects on peripheral immune cells, especially bone marrow-derived macrophages, in the context of PLX5622 have been debated as well[44]. Apart from its better performance in our study, PLX3397 has been approved by the US Food and Drug Administration for the treatment of tenosynovial giant cell tumours, which highlights the translational potential of this drug[45].

Few previous studies have investigated the general impact of irradiation on CNS myeloid cells. In a CCR2 reporter mouse model, irradiation led to early appearance of labelled cells in the brain, which was interpreted as infiltration of peripheral cells[46]. By contrast, a different study did not detect an increase in $CD11b^{+}CD45^{high}$ cells several weeks after irradiation, which was interpreted as a lack of peripheral cell engraftment, but the authors described a gene expression signature change with downregulation of homeostatic marker genes attributed to alterations in the naive microglia state[47]. In the context of our current study, these reports may support the hypothesis that irradiation primes the brain environment for repopulation with exogenous cells but by itself is insufficient to recruit cells from the periphery to the brain[46]. Similarly, a previous protocol used myeloablative whole-body irradiation with subsequent rescue systemic bone marrow transplantation with transgenic donor cells (*Cx3cr1*-CreER::DTA) to inhibit engraftment before intracranial injection of the microglial cell graft[20]. Despite the complexity of the approach, it resulted in only partial microglia replacement restricted to areas adjacent to the injection site.

A previous pioneering study investigating the ICV route for CNS myeloid replacement with whole-bone marrow cells reported—similar to our findings—a low level of brain chimerism of around 5% after 45 days if mice were preconditioned with lethal irradiation alone, which was followed by a continuous increase in the level of chimerism up to around 35% after 180 days[18]. Likewise, busulfan conditioning alone yielded only moderate early brain chimerism at a level of around 10% after 12 days, which increased to around 60% after 180 days. We demonstrate that the addition of transient depletion of endogenous microglia enables higher engraftment only a few weeks after transplantation. Notably, the previous study described the presence of donor-derived cells at low numbers in the femur bone marrow several hours after transplantation but not after 4 days[18]. In contrast to these observations with whole-bone marrow cells, we found repeatedly relevant engraftment in the peripheral haematopoietic system with HSPCs as donor cells, which is explainable by a higher number of KSL cells and potential long-term HSCs. Variability in the extent of peripheral engraftment in our experiment might have been due to heterogeneity in the donor cell population or procedure-related leakage into the vasculature or skull bone marrow in some mice.

This observation led us to further investigate the contribution of various haematopoietic subpopulations. We found that, contrary to previous notions, HSCs have little capacity for myeloid niche repopulation in vitro and are not required for CNS repopulation in vivo. Instead, we observed that CMPs have the strongest potential to repopulate microglia, in line with the finding that microglia originate from primitive Kit^{+} erythro-myeloid progenitors[4]. Taking advantage of this insight, we were able to further increase the brain specificity of our approach by depleting donor cells of cells expressing the Sca1 marker.

Inspired by the resulting almost complete lack of graft-derived cells in the blood circulation, we explored whether our microglia replacement approach could be used for allogeneic transplantation. As expected, we did not find any evidence of a graft-versus-host reaction. We were able to prevent early graft rejection using a peri-transplantation co-stimulation blockade regimen[35]. Although we found no rejection reaction up to around 1 month after ICV transplantation, graft cells were still present in most but not all mice after around 3 months and the degree of remaining engraftment was variable. Certainly, our experiments confirm that the brain is not an unequivocally immune-privileged organ. Nevertheless, the survival of transplanted fetal midbrain cells in patients with Parkinson's disease for up to 14 years, which was supported with peri- and post-transplantation 6-month immunosuppression using cyclosporin, indicates the overall practicability of allogeneic cell therapies for the human brain and emphasizes the necessity for adequate immune modulation[48]. Likewise, CNS myeloid cell engraftment derived from allogeneic HCT has recently been reported in human post-mortem tissue, hence further supporting the general translational feasibility of allogeneic CNS myeloid cell replacement[6,22]. In summary, our data provide proof of concept for the CNS engraftment of allogeneic haematopoietic cells and support future investigations to identify optimal immunosuppressive regimens for improved long-term myeloid graft survival.

We evaluated the gene therapeutic potential of our brain-specific myeloid cell replacement strategy in a mouse model of Sandhoff disease. This monogenic lysosomal storage disease with a neurodegenerative phenotype is a well-established model for evaluation of gene therapies, including the transplantation of different types of graft cells systemically (whole-bone marrow cells and human $CD34^{+}$ cells)[38,49] or intracranially (neural stem cells)[50]. Although CNS-grafted myeloid cells express lower levels of *Hexb* than endogenous microglia, our results show that they are sufficient to achieve a therapeutic effect[3]. Despite the varying extent of allograft persistence around 3 months after transplantation, we found profound improvements in behaviour and survival of treated mice. Although non-responder mice with premature death before 18 weeks were devoid of donor-derived brain myeloid cells, we still observed good functional outcomes in one mouse without any remaining graft cells as well as robust prevention of hippocampal glycolipid accumulation in several mice with a low level of donor chimerism at 18 weeks of age, suggesting that the effects of enzyme function restoration outlast the presence of grafted myeloid cells.

In the brain, *Hexb* mRNA is almost exclusively expressed in microglia. Unexpectedly, therefore, we observed prominent β-hexosaminidase activity in neurons in wild-type and transplanted knockout mice, which was especially apparent in the hippocampus and neocortex. This finding strongly suggests that grafted myeloid cells directly deliver HEXB to adjacent neurons, thereby restoring lysosomal function in $Hexb^{-/-}$ neurons and rescuing neurodegeneration. This HEXB transfer seems to be more efficient from endogenous microglia because grafted myeloid cells in $Hexb^{-/-}$ brains showed relatively more enzyme activity than microglia in wild-type mice. This finding implies that microglia contribute to the normal lysosomal function of neurons. Given the absence of donor cells in the peripheral circulation, our study provides evidence that locally engrafted myeloid cells are the main driver of disease rescue, as has been postulated in the context of systemic HCT[2]. The smaller treatment effects of bone marrow transplantation are most likely due to the less efficient, slow and variable nature of microglia replacement with this regimen[3]. Excitingly, the therapeutic potential of microglia replacement in Sandhoff disease has been independently confirmed in a recent study using primary mouse microglia as donor cells[51]. Furthermore, microglia replacement seems to also hold therapeutic potential for other neuro-destructive diseases, as recently demonstrated in patients with CSF1R-associated microgliopathy[52].

Allogeneic grafts have the potential to rescue gene dysfunction without the need for genetic engineering or gene delivery. This eliminates

safety concerns associated with genetic engineering[53–55] and increases the affordability and availability of cell therapies. Moreover, allogeneic transplantation would enable the use of off-the-shelf cell products, thus simplifying the manufacturing and distribution process while improving standardization for prospective patient care, which would also support certain applications that might depend on gene editing.

This is highlighted by our findings that human myeloid progenitor cells maintained the ability to engraft in the adult brain. Previous studies have demonstrated the ability of human ES cell- or induced pluripotent stem cell-derived myeloid cells to engraft in the neonatal mouse brain with variable efficency[56–59]. However, robust higher-level incorporation of human myeloid cells into the adult mouse brain required genetic engineering of donor cells to endow them with a competitive growth advantage[12].

In conclusion, our study demonstrates that rapid, high-efficiency replacement of brain myeloid cells is achievable without invasive manipulation of the global haematopoietic system and is applicable in an allogeneic setting. Our data suggest that brain-restricted myeloid cell therapy may be effective for neurotropic lysosomal storage disorders.

Online content

Any methods, additional references, Nature Portfolio reporting summaries, source data, extended data, supplementary information, acknowledgements, peer review information; details of author contributions and competing interests; and statements of data and code availability are available at https://doi.org/10.1038/s41586-025-09461-6.

1. Biffi, A. et al. Gene therapy of metachromatic leukodystrophy reverses neurological damage and deficits in mice. *J. Clin. Invest.* **116**, 3070–3082 (2006).
2. Capotondo, A. et al. Brain conditioning is instrumental for successful microglia reconstitution following hematopoietic stem cell transplantation. *Proc. Natl Acad. Sci. USA* **109**, 15018–15023 (2012).
3. Shibuya, Y. et al. Treatment of a genetic brain disease by CNS-wide microglia replacement. *Sci. Transl. Med.* **14**, eabl9945 (2022).
4. Kierdorf, K. et al. Microglia emerge from erythromyeloid precursors via Pu.1- and Irf8-dependent pathways. *Nat. Neurosci.* **16**, 273–280 (2013).
5. Masuda, T. et al. Spatial and temporal heterogeneity of mouse and human microglia at single-cell resolution. *Nature* **566**, 388–392 (2019).
6. Sankowski, R. et al. Multiomic spatial landscape of innate immune cells at human central nervous system borders. *Nat. Med.* **30**, 186–198 (2024).
7. Erblich, B., Zhu, L., Etgen, A. M., Dobrenis, K. & Pollard, J. W. Absence of colony stimulation factor-1 receptor results in loss of microglia, disrupted brain development and olfactory deficits. *PLoS ONE* **6**, e26317 (2011).
8. Elmore, M. R. P. et al. Colony-stimulating factor 1 receptor signaling is necessary for microglia viability, unmasking a microglia progenitor cell in the adult brain. *Neuron* **82**, 380–397 (2014).
9. Huang, Y. et al. Repopulated microglia are solely derived from the proliferation of residual microglia after acute depletion. *Nat. Neurosci.* **21**, 530–540 (2018).
10. Bennett, F. C. et al. A combination of ontogeny and CNS environment establishes microglial identity. *Neuron* **98**, 1170–1183 (2018).
11. Cronk, J. C. et al. Peripherally derived macrophages can engraft the brain independent of irradiation and maintain an identity distinct from microglia. *J. Exp. Med.* **215**, 1627–1647 (2018).
12. Chadarevian, J. P. et al. Engineering an inhibitor-resistant human CSF1R variant for microglia replacement. *J. Exp. Med.* **220**, e20220857 (2023).
13. Ajami, B., Bennett, J. L., Krieger, C., Tetzlaff, W. & Rossi, F. M. V. Local self-renewal can sustain CNS microglia maintenance and function throughout adult life. *Nat. Neurosci.* **10**, 1538–1543 (2007).
14. Priller, J. et al. Targeting gene-modified hematopoietic cells to the central nervous system: use of green fluorescent protein uncovers microglial engraftment. *Nat. Med.* **7**, 1356–1361 (2001).
15. Kierdorf, K., Katzmarski, N., Haas, C. A. & Prinz, M. Bone marrow cell recruitment to the brain in the absence of irradiation or parabiosis bias. *PLoS ONE* **8**, e58544 (2013).
16. Mildner, A. et al. Microglia in the adult brain arise from Ly-6C^{hi}CCR2^{+} monocytes only under defined host conditions. *Nat. Neurosci.* **10**, 1544–1553 (2007).
17. Wilkinson, F. L. et al. Busulfan conditioning enhances engraftment of hematopoietic donor-derived cells in the brain compared with irradiation. *Mol. Ther.* **21**, 868–876 (2013).
18. Capotondo, A. et al. Intracerebroventricular delivery of hematopoietic progenitors results in rapid and robust engraftment of microglia-like cells. *Sci. Adv.* **3**, e1701211 (2017).
19. Hohsfield, L. A. et al. Effects of long-term and brain-wide colonization of peripheral bone marrow-derived myeloid cells in the CNS. *J. Neuroinflammation* **17**, 279 (2020).
20. Xu, Z. et al. Efficient strategies for microglia replacement in the central nervous system. *Cell Rep.* **32**, 108041 (2020).
21. Sailor, K. A. et al. Hematopoietic stem cell transplantation chemotherapy causes microglia senescence and peripheral macrophage engraftment in the brain. *Nat. Med.* **28**, 517–527 (2022).
22. Loeb, A. M., Pattwell, S. S., Meshinchi, S., Bedalov, A. & Loeb, K. R. Donor bone marrow-derived macrophage engraftment into the central nervous system of patients following allogeneic transplantion. *Blood Adv.* **7**, 5851–5859 (2023).
23. Mader, M. M.-D. et al. Myeloid cell replacement is neuroprotective in chronic experimental autoimmune encephalomyelitis. *Nat. Neurosci.* **27**, 901–912 (2024).
24. Yoo, Y., Neumayer, G., Shibuya, Y., Mader, M. M.-D. & Wernig, M. A cell therapy approach to restore microglial Trem2 function in a mouse model of Alzheimer's disease. *Cell Stem Cell* **30**, 1043–1053 (2023).
25. Eichler, F. et al. Hematopoietic stem-cell gene therapy for cerebral adrenoleukodystrophy. *N. Engl. J. Med.* **377**, 1630–1638 (2017).
26. Yoon, I. C., Bascou, N. A., Poe, M. D., Szabolcs, P. & Escolar, M. L. Long-term neurodevelopmental outcomes of hematopoietic stem cell transplantation for late-infantile Krabbe disease. *Blood* **137**, 1719–1730 (2021).
27. Gentner, B. et al. Hematopoietic stem- and progenitor-cell gene therapy for Hurler syndrome. *N. Engl. J. Med.* **385**, 1929–1940 (2021).
28. Fumagalli, F. et al. Lentiviral haematopoietic stem-cell gene therapy for early-onset metachromatic leukodystrophy: long-term results from a non-randomised, open-label, phase 1/2 trial and expanded access. *Lancet* **399**, 372–383 (2022).
29. Boucher, A. A. et al. Long-term outcomes after allogeneic hematopoietic stem cell transplantation for metachromatic leukodystrophy: the largest single-institution cohort report. *Orphanet J. Rare Dis.* **10**, 94 (2015).
30. Aldenhoven, M. et al. Long-term outcome of Hurler syndrome patients after hematopoietic cell transplantation: an international multicenter study. *Blood* **125**, 2164–2172 (2015).
31. Simard, A. R., Soulet, D., Gowing, G., Julien, J.-P. & Rivest, S. Bone marrow-derived microglia play a critical role in restricting senile plaque formation in Alzheimer's disease. *Neuron* **49**, 489–502 (2006).
32. Mishra, P. et al. Rescue of Alzheimer's disease phenotype in a mouse model by transplantation of wild-type hematopoietic stem and progenitor cells. *Cell Rep.* **42**, 112956 (2023).
33. Bryder, D., Rossi, D. J. & Weissman, I. L. Hematopoietic stem cells: the paradigmatic tissue-specific stem cell. *Am. J. Pathol.* **169**, 338–346 (2006).
34. Getts, D. R. et al. Ly6c^{+} "inflammatory monocytes" are microglial precursors recruited in a pathogenic manner in West Nile virus encephalitis. *J. Exp. Med.* **205**, 2319–2337 (2008).
35. Li, S. et al. Induction of immunological tolerance to myelinogenic glial-restricted progenitor allografts. *Brain* **142**, 3456–3472 (2019).
36. Lightbourn, C. O. et al. Use of post-transplant cyclophosphamide treatment to build a tolerance platform to prevent liquid and solid organ allograft rejection. *Front. Immunol.* **12**, 636789 (2021).
37. Sango, K. et al. Mouse models of Tay–Sachs and Sandhoff diseases differ in neurologic phenotype and ganglioside metabolism. *Nat. Genet.* **11**, 170–176 (1995).
38. Norflus, F. et al. Bone marrow transplantation prolongs life span and ameliorates neurologic manifestations in Sandhoff disease mice. *J. Clin. Invest.* **101**, 1881–1888 (1998).
39. Spangenberg, E. et al. Sustained microglial depletion with CSF1R inhibitor impairs parenchymal plaque development in an Alzheimer's disease model. *Nat. Commun.* **10**, 3758 (2019).
40. Najafi, A. R. et al. A limited capacity for microglial repopulation in the adult brain. *Glia* **66**, 2385–2396 (2018).
41. Hohsfield, L. A. et al. Subventricular zone/white matter microglia reconstitute the empty adult microglial niche in a dynamic wave. *eLife* **10**, e66738 (2021).
42. Claeys, W. et al. Limitations of PLX3397 as a microglial investigational tool: peripheral and off-target effects dictate the response to inflammation. *Front. Immunol.* **14**, 1283711 (2023).
43. Okojie, A. K. et al. Distinguishing the effects of systemic CSF1R inhibition by PLX3397 on microglia and peripheral immune cells. *J. Neuroinflammation* **20**, 242 (2023).
44. Lei, F. et al. CSF1R inhibition by a small-molecule inhibitor is not microglia specific; affecting hematopoiesis and the function of macrophages. *Proc. Natl Acad. Sci. USA* **117**, 23336–23338 (2020).
45. Tap, W. D. et al. Pexidartinib versus placebo for advanced tenosynovial giant cell tumour (ENLIVEN): a randomised phase 3 trial. *Lancet* **394**, 478–487 (2019).
46. Morganti, J. M., Jopson, T. D., Liu, S., Gupta, N. & Rosi, S. Cranial irradiation alters the brain's microenvironment and permits CCR2^{+} macrophage infiltration. *PLoS ONE* **9**, e93650 (2014).
47. Voshart, D. C. et al. Radiotherapy induces persistent innate immune reprogramming of microglia into a primed state. *Cell Rep.* **43**, 113764 (2024).
48. Mendez, I. et al. Dopamine neurons implanted into people with Parkinson's disease survive without pathology for 14 years. *Nat. Med.* **14**, 507–509 (2008).
49. Beegle, J., Hendrix, K., Maciel, H., Nolta, J. A. & Anderson, J. S. Improvement of motor and behavioral activity in Sandhoff mice transplanted with human CD34^{+} cells transduced with a HexA/HexB expressing lentiviral vector. *J. Gene Med.* **22**, e3205 (2020).
50. Lee, J.-P. et al. Stem cells act through multiple mechanisms to benefit mice with neurodegenerative metabolic disease. *Nat. Med.* **13**, 439–447 (2007).
51. Chen, D. et al. Brain-wide microglia replacement using a nonconditioning strategy ameliorates pathology in mouse models of neurological disorders. *Sci. Transl. Med.* **17**, eads6111 (2025).
52. Wu, J. et al. Microglia replacement halts the progression of microgliopathy in mice and humans. *Science* **389**, eadr1015 (2025).
53. Doudna, J. A. The promise and challenge of therapeutic genome editing. *Nature* **578**, 229–236 (2020).
54. Sabatino, D. E. et al. Evaluating the state of the science for adeno-associated virus integration: an integrated perspective. *Mol. Ther.* **30**, 2646–2663 (2022).
55. Goyal, S. et al. Acute myeloid leukemia case after gene therapy for sickle cell disease. *N. Engl. J. Med.* **386**, 138–147 (2022).

56. Mancuso, R. et al. Stem-cell-derived human microglia transplanted in mouse brain to study human disease. *Nat. Neurosci.* **22**, 2111–2116 (2019).
57. Hasselmann, J. et al. Development of a chimeric model to study and manipulate human microglia in vivo. *Neuron* **103**, 1016–1033 (2019).
58. Svoboda, D. S. et al. Human iPSC-derived microglia assume a primary microglia-like state after transplantation into the neonatal mouse brain. *Proc. Natl Acad. Sci. USA* **116**, 25293–25303 (2019).
59. Xu, R. et al. Human iPSC-derived mature microglia retain their identity and functionally integrate in the chimeric mouse brain. *Nat. Commun.* **11**, 1577 (2020).

Publisher's note Springer Nature remains neutral with regard to jurisdictional claims in published maps and institutional affiliations.

Springer Nature or its licensor (e.g. a society or other partner) holds exclusive rights to this article under a publishing agreement with the author(s) or other rightsholder(s); author self-archiving of the accepted manuscript version of this article is solely governed by the terms of such publishing agreement and applicable law.

© The Author(s), under exclusive licence to Springer Nature Limited 2025

Methods

Animal experiments

All animal procedures were approved by the administrative panel on laboratory animal care at Stanford University (APLAC21565). Mice were group housed (up to five mice per cage) on a 12-h light/12-h dark cycle. Water and standard chow were provided ad libitum unless otherwise described. The ambient temperature was 20–22 °C, and the humidity was 20–80%. Female mice were used for experiments unless otherwise stated. Experimental animals were 6–13 weeks old at the time of cell transplantation unless otherwise specified. Mice were randomly assigned to experimental groups, controlling for sex where applicable. Sample sizes were estimated based on existing literature and/or empirical knowledge.

The following mouse strains were used: C57BL/6J mice (JAX, strain 000664; referred to in this paper as C57BL/6) were used as host animals for transplantation studies and to generate primary glial cultures. The C57BL/6-Tg(UBC-GFP)30Scha/J strain (JAX, strain 004353)[60] was crossed with wild-type C57BL/6 mice to generate hemizygote B6.UBC-GFP mice. Hemizygote B6.UBC-GFP mice were used as donor animals to collect haematopoietic cells. CSF1R-knockout mice (FVB.129×1-Csf1r^{tm1Ers}; crossing *Csf1r*$^{+/-}$ with *Csf1r*$^{+/-}$ mice to obtain *Csf1r*$^{-/-}$ mice; a gift from R. Stanley (Albert Einstein College of Medicine))[10,61] were used for primary glia generation. B6.KUO mice (C57BL/6 background; generated at the University of Tokyo and a gift from H. Nakauchi) express the fluorescent protein KUO in the haematopoietic lineage and were used to collect haematopoietic cells[62]. The HEXB-knockout strain was obtained from JAX (B6;129S-Hexb^{tm1Rlp}/J; strain 002914)[37], and heterozygous animals (*Hexb*$^{+/-}$) were used as breeders. The colony was maintained as a mixed-background strain (B6;129S). For allogeneic transplantation studies to evaluate engraftment and rejection of donor cells, wild-type (*Hexb*$^{+/+}$) or heterozygous (*Hexb*$^{+/-}$) mice were used as hosts. As a disease model of Sandhoff disease, homozygous-knockout recipient mice (*Hexb*$^{-/-}$) were used. FVB/NJ mice (JAX, strain 001800; referred to in this paper as FVB) were used as host animals for transplantation studies. Immunodeficient mice with expression of human CSF1 (referred to as *Il2rg*$^{-/-}$*Rag2*$^{-/-}$h*CSF1*$^{+/+}$ mice; C;129S4-Rag2$^{tm1.1Flv}$ Csf1$^{tm1(CSF1)Flv}$Il2rg$^{tm1.1Flv}$/J; JAX, strain 017708)[63] were used as host animals for xenograft transplantation.

Genotyping

Genomic DNA was extracted from mouse tissue using QuickExtract DNA extraction solution (Lucigen/LGC, Biosearch Technologies). The transgenic loci were amplified by PCR (Phusion High-Fidelity DNA Polymerase, NEB) and evaluated by agarose gel electrophoresis. The following transgene-specific assays were used.

Primer set for *Hexb*: F1, 5′-ATTTTAAAATTCAGGCCTCGA-3′; R1, 5′-CATTCTGCAGCGGTGCACGGC-3′; R2, 5′-CATAGCGTTGGCTACC CGTGA-3′. Touchdown thermocycler programme for *Hexb*: (1) 98 °C for 2 min; (2) 98 °C for 10 s; (3) 65 °C (−0.5 °C per cycle, 30 s); (4) 72 °C for 30 s; (5) repeat steps 2–4 for 10 cycles; (6) 98 °C for 10 s; (7) 60 °C for 30 s; (8) 72 °C for 30 s; (9) repeat steps 6–8 for 28 cycles; and (10) 72 °C for 10 min. Expected bands (*Hexb*): F1/R1 for wild type, ~100 bp; F1/R2 for mutant, ~200 bp.

Primer set for CSF1R knockout: F1, 5′-AGACTCATTCCAGAAC CAGAGC-3′; F2, 5′-CCGGTAGAATTCCTCGAGTCTA-3′; R1, 5′-GAATT TGGAGTCCTCACCTTTG-3′. Touchdown thermocycler programme for CSF1R knockout: (1) 94.0 °C for 2 min; (2) 94 °C for 20 s; (3) 65 °C (−0.5 °C per cycle) for 15 s; (4) 68 °C for 10 s; (5) repeat steps 2–4 for 10 cycles; (6) 94 °C for 15 s; (7) 60 °C for 15 s; (8) 72 °C for 10 s; (9) repeat steps 6–8 for 28 cycles; and (10) 72 °C for 2 min. Expected bands (CSF1R knockout): F1/R1 for wild type, ~400 bp; F2/R1 for mutant, ~350 bp.

Genotype for KUO was determined by flow cytometry assessment (PE channel) of blood cells. The genotype of UBC-GFP mice was determined with fluorescent light and later confirmed by flow cytometry analysis of haematopoietic cells.

All primers were ordered from IDT.

HSPC culture

HSPC cultures were generated and maintained as previously described in detail[64,65]. In brief, the femur, tibia, ilium and spinal column of donor mice were dissected and whole-bone marrow cells were extracted. Cells were stained with APC-conjugated anti-c-Kit antibody (Invitrogen, 17-1171-83) and subsequently incubated with anti-APC MACS beads (Miltenyi Biotec, 130-090-855). Kit$^+$ cells were enriched through MACS using a QuadroMACS instrument with LS columns (Miltenyi Biotec, 130-042-401). Subsequently, cells from the positive fraction were first stained with a biotin-conjugated lineage antibody mix (Miltenyi Biotec, 130-090-858; 1:100) and then stained with fluorophore-conjugated antibodies (see 'Flow cytometry' section below for a list of antibodies) followed by propidium iodide as live stain (Invitrogen, P3566). Long-term HSCs used for ex vivo expansion were defined as Lin$^-$Kit$^+$ Sca1$^+$CD150$^+$CD48$^-$ and isolated through fluorescence-activated cell sorting (FACS) with a BD FACSAria II. Sorted cells were maintained in HSC medium (F-12 (Gibco, 11765054) supplemented with GlutaMAX (Gibco, 35050061), HEPES (Gibco, 15630080), penicillin/streptomycin (Gibco, 15140163), insulin-transferrin-selenium-ethanolamine (Gibco, 51500056), poly(vinyl alcohol) (Sigma-Aldrich, P8136), mouse stem cell factor (SCF; PeproTech, AF-250-03) and mouse thrombopoietin (TPO; PeproTech, AF-315-14 or Gibco, RP-87753)) in fibronectin-coated or CellBIND plates (Corning) in cell culture incubators with 5% CO_2 and 5% O_2 at 37 °C. The medium was changed every 2 days.

Depletion of Sca1$^+$ HSPCs

Depletion was performed with an anti-Sca1 MicroBead kit (Miltenyi Biotec, 130-123-124) according to the manufacturer's instructions. In brief, HSPCs were first stained with a Vio Bright FITC-conjugated anti-Sca1 antibody and subsequently stained with anti-FITC MicroBeads. Stained cells were depleted with MACS using a QuadroMACS instrument with LD columns (Miltenyi Biotec, 130-042-901). Optionally, HSPC cultures were moved to a cell culture incubator with 5% CO_2 and 21% O_2 at 37 °C for 5–7 days before the depletion procedure.

Culture of primary glia

Forebrains were collected from newborn (postnatal day 2–3) mice. Brain homogenates were digested with trypsin-EDTA (0.25%; Gibco, 25200056) and cultured in glia medium (DMEM (Gibco, 12430054) supplemented with non-essential amino acids (NEAA; Gibco, 11140050), sodium pyruvate (Gibco, 11360070), penicillin/streptomycin (Gibco, 15140163), 2-mercaptoethanol (Sigma-Aldrich, M6250) and 10% Cosmic calf serum (CCS; HyClone). Cultures were maintained in cell culture incubators with 5% CO_2 and 21% O_2 at 37 °C. The medium was changed every 7 days. Cells were split by trypsin dissociation.

Culture of HSPC-derived myeloid cells

In vitro HSPC-derived myeloid cells were generated by co-culturing HSPCs with primary glia. Primary glia were plated in tissue culture treated plates (Falcon) in glia medium (see above) and maintained in monoculture until confluent. Depending on the experiment (see figure captions), either C57BL/6 or CSF1R-knockkout primary glia were used. Endogenous microglia in C57BL/6 primary glia were depleted using PLX5622 (MedChemExpress, HY-114153) at a concentration of 250 nM for around 1 week. The medium was then changed to MG medium (DMEM/F12 (Gibco, 11320082) supplemented with NEAA (Gibco, 11140050), sodium pyruvate (Gibco, 11360070) and penicillin/streptomycin (Gibco, 15140163)) supplemented with 10% fetal bovine serum (Atlanta Biologicals) unless otherwise described in the figure legend. Graft cells were plated onto the glial cell layer by FACS at a density of 100 cells per 1.9 cm^2 per population using a BD FACSAria II. Cultures were

maintained in cell culture incubators with 5% CO_2 and 21% O_2 at 37 °C. Medium changes were performed by replacing 50% of the MG medium every third day. On the day of analysis indicated in the figure legends, the culture was collected using trypsin dissociation and prepared for flow cytometry analysis (see below).

Generation of human ES cell-derived myeloid progenitor cells

Human ES cell experiments were approved by the stem cell research oversight panel at Stanford University. H1 ES cells (originally obtained from WiCell Research Resources; cells were regularly evaluated for morphology and growth characteristics (no additional authentication was performed); cells were regularly monitored for mycoplasma contamination) were genetically modified to express GFP by targeting the *CLYBL* locus with a CAGGS-GFP expression cassette and maintained without feeder cells in StemFlex medium (Gibco). Myeloid differentiation was induced as previously described[66]. In brief, embryonic bodies were generated in mTeSR-1 medium (STEMCELL Technologies) supplemented with 50 ng ml^{-1} bone morphogenetic protein 4, 50 ng ml^{-1} vascular endothelial growth factor and 20 ng ml^{-1} SCF (PeproTech) for 4 days. Differentiation was then promoted by culture in Diff medium (X-Vivo15 medium (Lonza) with GlutaMAX (Gibco) and 2-mercaptoethanol (Sigma-Aldrich)) supplemented with 50 ng ml^{-1} SCF, 50 ng ml^{-1} macrophage colony-stimulating factor (M-CSF), 50 ng ml^{-1} interleukin-3, 50 ng ml^{-1} FLT3 and 5 ng ml^{-1} TPO (PeproTech) for 1 week. The medium was then changed weekly to Diff medium supplemented with 50 ng ml^{-1} FLT3, 50 ng ml^{-1} M-CSF and 25 ng ml^{-1} granulocyte–macrophage colony-stimulating factor (PeproTech). Cells were collected, filtered through a 70-µm cell strainer, enriched for CD14 expression using MACS (CD14 MicroBeads, human, Miltenyi) and resuspended in PBS for transplantation on day 24 of the protocol.

Busulfan conditioning and systemic injection of haematopoietic cells

Busulfan (Sigma-Aldrich, B2635) was applied i.p. with a daily dose of 25 mg kg^{-1}. A working solution of 1 mg ml^{-1} was prepared fresh every day from a DMSO stock solution of 49 mg ml^{-1} by dilution with PBS. The number of treatment days is indicated in the figures or figure legends.

Rescue bone marrow transplantation. Depending on the experimental design (as indicated in the figures and figure legends), 2×10^5 fresh whole-bone marrow cells in 200 µl PBS were retro-orbitally injected 3–5 days after ICV transplantation to rescue mice from mortality caused by myeloablation.

Therapeutic bone marrow transplantation. As a treatment regimen in *Hexb*$^{-/-}$ mice, 8 million fresh whole-bone marrow cells in 200 µl PBS were retro-orbitally injected after 5 days of daily busulfan injection.

In vivo CSF1R inhibitor treatment

PLX5622 for diet application was provided by Plexxikon under a material transfer agreement and incorporated into AIN-76A standard chow by Research Diets at 1,200 parts per million. Mice were given a PLX5622-containing diet ad libitum for 14 or 25 days as indicated.

PLX5622 hemifumarate was used for i.p. injections and was purchased from MedChemExpress (HY-114153A). It was dissolved in DMSO at a concentration of 200 mM as a stock solution. A suspension of the stock solution with PBS + 1% polysorbate 80 (Sigma-Aldrich, 59924) was made for injections using vortexing and sonication. The daily dose was 200 mg kg^{-1}.

PLX3397 was purchased from MedChemExpress (pexidartinib, HY-16749) and was dissolved in DMSO at a concentration of 100 mM as a stock solution. A suspension of the stock solution with PBS + 1% polysorbate 80 (Sigma-Aldrich, 59924) was prepared for injections with vortexing. Mice were injected with 184 mg kg^{-1} daily, except for the *Il2rg*$^{-/-}$*Rag2*$^{-/-}$h*CSF1*$^{+/+}$ mouse strain, for which a daily dose of 92 mg kg^{-1} was used.

Head-specific irradiation

Irradiation was performed with a Kimtron Polaris MC-500 X-ray system. Mice were placed in a restrainer with a body irradiation shield (Braintree Scientific) for head-specific exposure. Irradiation doses stated in this study are the actual doses received by the mice, which were achieved after delivering a corrected dose calibrated for the restrainer.

Immunomodulatory regimens

Co-stimulation blockade[35,67] was induced by i.p. injection of InVivoMAb anti-mouse CD40L (CD154; 500 µg per injection; BioXCell) and InVivoMAb recombinant CTLA-4–Ig (hum/hum; 500 µg per injection; BioXCell) diluted in InVivoPure pH 7.0 dilution buffer (total volume of 300 µl per injection; BioXCell). Injections were performed on the day of transplantation as well as on postoperative days 2, 4 and 6. Where indicated in the figure legends, additional booster injections were performed every 2 weeks after transplantation.

Cyclophosphamide (cyclophosphamide monohydrate, Calbiochem/MilliporeSigma; refs. 36,68–70) was injected i.p. with a dose of 200 mg kg^{-1} diluted in PBS with a concentration of 10 mg ml^{-1}. Recipient mice were retro-orbitally injected with 10 million splenocytes (7 days before ICV transplantation), 0.5 million HSPCs (7 days before ICV transplantation) or a combination of 10 million whole-bone marrow cells and 30 million splenocytes (after irradiation; 4 days before ICV transplantation). Cells were derived from B6.UBC-GFP mice and were suspended in PBS for injection. The spleen was mechanically dissociated by passing it through a 70-µm cell strainer. Whole-bone marrow cells and splenocytes were incubated in red blood cell lysis buffer for 10 min[71] and filtered through a 70-µm cell strainer. Cyclophosphamide was injected 3 days after the cell injections.

ICV injections

Recipient mice were anaesthetized with ketamine (VetaKet/Ketaset, Zoetis) and xylazine (AnaSed). The head was shaved, the animal was placed in a stereotactic frame, the skin was disinfected and the skull was exposed through a midline incision. A burr hole was placed over the injection site, and the following coordinates were used for stereotactic injection: 1.0 mm lateral, 0.4 mm posterior, 2.0 mm ventral. For the *Il2rg*$^{-/-}$*Rag2*$^{-/-}$h*CSF1*$^{+/+}$ mouse strain, this was adapted to 3.0 mm ventral and burr holes were placed bilaterally. Cells were injected in PBS at a concentration of 100,000 cells per µl in a microsyringe (Hamilton) using a microinjector. The injection speed was 0.5 µl min^{-1}. After injection, the needle was left in place for 2 min and was then slowly retracted. The burr hole was closed with bone wax (CP Medical), followed by closure of the wound. For postoperative pain management, carprofen (Rimadyl, Zoetis) was administered.

Behavioural tests and clinical assessment

All behavioural assessments were performed with blinding to treatment group. Tests were performed at consistent times of day, with only one type of test performed per mouse per day. Mice were allowed to acclimatize in the testing room for a minimum of 30 min before assessment, and all testing rooms maintained a consistent and quiet environment away from other mice. All testing equipment was thoroughly cleaned with 70% ethanol and Virkon-S disinfectant between mice.

Rotarod test. Motor coordination was measured by rotarod testing. Testing was performed on a Med Associates ENV-575M rotarod treadmill on acceleration setting '2.0–20 RPM' with an acceleration of 0.06 rpm s^{-1}. Before the first day of testing, mice underwent a training session consisting of three trials. Performance on the rotarod was then evaluated at 10, 14 and 17 weeks of age. Mice were tested in three replicates with a 1-hour gap to rest between replicates. Mice were allowed to run freely on the rotarod until they fell off or reached the maximum time of 360 s. Latency to fall (in seconds) was recorded for

each session, and the three replicate times were averaged for each time point. If the mouse simply held on to the rod and did not take any steps for the duration of the test, the replicate was excluded from analysis. Deceased animals were scored with 0 s.

Open-field test. Video acquisition and analysis were performed using BIOBSERVE Viewer[3] software (version 3.0.1.442). Open-field activity was evaluated at 13 and 17 weeks of age and additionally at 22, 26 and 30 weeks of age in a long-term observation group. Four 40 × 40 cm^2 plywood boxes were placed in a 2 × 2 configuration in the centre of the testing room. After acclimatization, one mouse was placed in each box. Recording was started with a delay of 30 s, and the investigator left the room. A camera mounted overhead recorded mouse activity in the boxes for a period of 15 min. Video recordings of the first 5 min were then analysed with the Viewer tracking software, using the centre of the mouse's body as the reference point. Centre zones were defined as half the size of the box floor and located in the centre of the box area. Deceased animals were excluded from analysis.

Neuro score. The neuro score used in this study was adapted from a previously reported neurological scoring system[72]. Mice were evaluated weekly starting at 10 weeks of age. Mice were given a score from 0–3 in three areas (hindlimb clasping, gait and ledge walking), with 0 indicating an absence of neurological symptoms and 3 indicating the most severe presentation, for a total score out of 9. After acclimatization, mice were scored one at a time in fresh cages with a thin layer of bedding. The hindlimb clasping score was determined by holding the mouse by its tail above the testing cage for a period of 10 s. After 1 min, the test was repeated and the two scores were averaged. Gait scores were determined by observing the mouse's mobility, both inside the lined cage and on a flat absorbent pad placed on the workbench, for a period of at least 30 s. The ledge test was performed by placing the mouse on the edge of the testing cage and allowing it to walk freely along the ledge until it descended into the cage or refused to move. Scoring criteria are detailed in Extended Data Table 1. Mice were euthanized after they reached and maintained a maximum neuro score. Deceased animals received the maximum score of 9.

Body weight and condition. Body weight and body condition scores were recorded weekly starting at 10 weeks of age[73].

Graft-versus-host disease score. The likelihood of graft-versus-host disease in this study was evaluated with a score based on previously published clinical criteria[74,75] (Extended Data Table 1). Mice were evaluated weekly starting at 10 weeks of age and were given a score of 0–2 for five indicators of graft-versus-host disease: weight loss, hunched posture, alopecia, skin fibrosis and diarrhoea. Weight loss was calculated from the previous body weight measurement, indicating change over a 1-week period. Spinal curvature clearly resulting from hindlimb paralysis was not counted as hunched posture. Alopecia was only considered if it occurred outside the irradiation field, to exclude instances of irradiation-induced hair loss. Notably, not all criteria for the score were specific to the presence of graft-versus-host disease in our study. We also observed the presence of alopecia in non-transplanted mice in the investigated mouse strain. Hunching and weight loss were also features of the neurological phenotype of HEXB deficiency.

Exclusions from analysis in the *Hexb* cohorts. Mice with periprocedural mortality were excluded from the analysis. One CT mouse was found dead on day 114 (presence of GFP^+ cells in the brain confirmed post-mortem; Extended Data Fig. 5g) under unclear circumstances, together with a wild-type cage mate, and was excluded from subsequent behaviour time points and the survival analysis.

Tissue collection from experimental mice for downstream analysis

Mice were deeply anaesthetized with Avertin (Sigma-Aldrich, T48402)[76]. Peripheral blood was collected from the retro-orbital plexus using heparin-coated glass capillary tubes (Fisher Scientific, 22-260950). Mice were then transcardially perfused with ice-cold PBS without Ca^{2+} or Mg^{2+}. Afterwards, if applicable, leg bones or skull bones were collected for bone marrow extraction as described above. Brains were collected.

In selected mice that were found dead, a necropsy was performed to dissect the brain.

Flow cytometry

Brains were first minced with a razor blade and then transferred to ice-cold HBSS without Ca^{2+} or Mg^{2+} (Gibco). The tissue was then enzymatically dissociated using Neural Tissue Dissociation Kit P (Miltenyi Biotec) in accordance with the manufacturer's protocol. The total incubation time at 37 °C was 35 min; afterwards, the tissue was kept on ice or at 4 °C. After washing with ice-cold HBSS (with Ca^{2+} and Mg^{2+}) and passage through a 70-µm cell strainer, gradient centrifugation was performed using a 30% Percoll/HBSS solution (Cytiva Percoll Centrifugation Media) at 700*g* for 10 min. The resulting cell pellet was washed with PBS, and cells were resuspended in flow buffer (PBS with 5% CCS) with antibodies for 20 min at 4 °C.

Peripheral blood was first incubated for 10 min in ice-cold red blood cell lysis buffer[71]. After washing in PBS, cells were resuspended in flow buffer with antibodies. Samples were incubated for 15–30 min at 4 °C depending on the panel.

The evaluation of peripheral blood immune cells including lymphocyte populations was adapted from ref. 77 using the following staining workflow. First, live/dead staining was performed using Zombie Red (BioLegend, 423109), and cells were then incubated with anti-mouse CD16/CD32 (Mouse BD Fc Block; BD, 553141); staining for surface antigens was then performed as described above. Subsequently, cells were fixed, permeabilized and intracellularly stained (True-Nuclear Transcription Factor Buffer Set).

Bone marrow cells were extracted as described above and optionally incubated in red blood cell lysis buffer. For staining, samples were first incubated with an antibody mix for lineage marker for 30 min at room temperature (Miltenyi Biotec, 130-090-858). Staining was then performed with other antibodies using an incubation time of 30–90 min depending on the panel used. Gating for haematopoietic cell subpopulations was based on previous publications[3,65,78].

In vitro samples were dissociated through incubation with trypsin for 5 min at 37 °C followed by quenching with flow buffer and were spun down. The cell pellet was resuspended in flow buffer with antibodies and incubated for 15 min at 4 °C.

For all samples, after incubation with antibodies, samples were washed with PBS and cell pellets were resuspended in flow buffer with live/dead stain for non-fixed samples and kept on ice for analysis.

Antibodies for the following markers were used: CD3e (clone 145-2C11; BioLegend, 100308/100353; 1:200), CD4 (clone GK1.5; BioLegend, 100414; 1:200), CD8a (clone 53-6.7; BioLegend, 100798; 1:200), CD11b (clone M1/70; BioLegend, 101208/101224/101236; 1:200), CD16/32 (clone 93; BioLegend, 101331; 1:300), CD19 (clone 6D5; BioLegend, 115520; 1:200), CD25 (clone PC61; BioLegend, 102036; 1:100), CD34 (clone RAM34; BD, 560518; 1:100), CD44 (clone IM7; BioLegend, 103059; 1:200), CD45 (clone 2D1; BioLegend, 368512; 1:20), CD45 (clone 30-F11; BioLegend, 103112/103128; 1:200), CD48 (clone HM48-1; BioLegend, 103428; 1:300), CD62L (clone MEL-14; BioLegend, 104411; 1:200), CD127 (clone SB/199; BioLegend, 121112; 1:300), CD150 (clone TC15-12F12.2; BioLegend, 115913; 1:300), FoxP3 (clone 150D; BioLegend, 320008; 1:50), c-Kit (clone 2B8; Invitrogen, 17-1171-83; 1:300), Ly6c (clone HK1.4; BioLegend, 128023; 1:300), NKp46 (clone 29A1.4; BioLegend, 137609; 1:100), Sca1 (clone D7; BioLegend, 108108 or BD, 563990; 1:300)

and streptavidin (BD, 554063; 1:300). For live/dead staining, DAPI (Sigma, D9542), propidium iodide (Invitrogen, P3566) or Zombie Red (BioLegend, 423109) was used.

Flow cytometry was performed on a BD FACSAria II or a BD CytoFLEX. Data analysis was performed using FlowJo software (version 10.8.1).

Histological processing, staining and microscopy

Tissues were fixed in 4% paraformaldehyde overnight and then transferred to 30% sucrose in PBS. Tissues were embedded in Tissue-Tek OCT compound (Sakura Finetek, 4583). Sections of either 20 µm or 40 µm in thickness were obtained using a cryostat (CM 3050S, Leica), with consistent thickness between experimental groups per stain. If not all samples in an experimental group were analysed, selection of samples was performed at random.

For immunofluorescence staining, the following primary antibodies were used: anti-GFP (Abcam, ab13970; 1:1,000), anti-IBA1 (FUJIFILM Wako, 019-19741; 1:1,000), anti-P2RY12 for mouse (BioLegend, 848002; 1:100), anti-P2RY12 for human (Sigma, HPA014518; 1:100), anti-TMEM119 for mouse (Abcam, ab209064; 1:500) and anti-TMEM119 for human (Invitrogen, PA5-62505; 1:100). Sections were washed in PBS and then incubated in IF buffer (PBS with 5% CCS and 0.3% Triton X-100 (Sigma-Aldrich)) for 1 h. Staining with primary antibody (diluted in IF buffer) was performed at 4 °C overnight. After washing three times with PBS, staining with secondary antibody (ThermoFisher; fluorophores included Alexa Fluor 488, 594 and 647; antibodies were diluted in IF buffer) was performed at room temperature for 1 h. After washing three times with PBS, sections were counterstained with DAPI (diluted in PBS) for 5 min. After washing in PBS, sections were mounted on glass slides with ProLong Gold antifade reagent (ThermoFisher, P36930).

In situ β-hexosaminidase determination was performed as previously described with the following adaptions (all steps at room temperature)[79]. In brief, 20-µm brain sections were mounted on glass slides (Fisherbrand Superfrost Plus), incubated in PBS with 0.01% Nonidet-P 40 (substitute solution; Sigma-Aldrich) for 15 min and washed three times in CP buffer (0.05 M citrate and 0.1 M phosphate, pH 4.5). Sections were then incubated for 1 h in β-hexosaminidase staining buffer (0.3 mg ml^{-1} naphthol AS-BI *N*-acetyl-β-D-glucosaminide (Sigma-Aldrich, N4006; dissolved in dimethylformamide, Sigma-Aldrich) and 1 mg ml^{-1} Fast Garnet GBC sulfate salt (Sigma-Aldrich, F8761; in CP buffer)). Sections were then washed four times in distilled water, blocked for 1 h in IF buffer and incubated for 1 h with anti-GFP primary antibody in IF buffer (Abcam, ab13970; 1:1,000; for CT samples, all other samples were incubated in IF buffer without antibody). Sections were then washed four times in distilled water, incubated in β-hexosaminidase staining buffer for another 2 h and washed four times with distilled water. Sections were incubated in IF buffer for 1 h with Alexa Fluor 488-conjugated secondary antibody (for CT samples; all other samples were incubated in IF buffer without antibody). Samples were washed in distilled water four times and coverslipped with ProLong Gold antifade reagent (ThermoFisher, P36930).

For PAS staining (Abcam, ab150680), 20-µm brain sections were mounted on glass slides (Fisherbrand Superfrost Plus) and stained following the manufacturer's instructions. In brief, sections were immersed in periodic acid solution for 5 min, washed, immersed in Schiff's solution for 15 min, washed, immersed in haematoxylin (modified Mayer's) for 2 min, washed, immersed in bluing reagent for 30 s, washed and coverslipped with mounting medium (Aqua-Mount, VWR).

Images were obtained using a Zeiss LSM980 confocal microscope with Airyscan 2, Zeiss AxioImager and Leica DM5500 B. For image acquisition, ZEN blue (Zeiss, version 3.7.97.04000 and version 3.8.99.03000) and Leica Application Suite X (Leica, 3.7.1.21655) software were used. ZEN blue software was used for Airyscan processing and stitching of tiled images. All other image postprocessing and analysis were performed using Fiji/ImageJ (NIH, version 1.54f) software.

Histological analysis

High-resolution tiled images for illustrative purposes were obtained by confocal Airyscan microscopy. Brightness and contrast were adjusted individually to optimize the signal-to-noise ratio.

For histological quantification of the engraftment efficiency of B6.UBC-GFP cells in *Hexb*$^{-/-}$ mice, tiled images of sagittal brain sections were obtained by confocal Airyscan microscopy for the GFP channel using consistent imaging parameters. After Airyscan postprocessing and stitching using ZEN blue, images were processed and analysed with Fiji/ImageJ: after 8-bit conversion, the cerebrum was selected (excluding the olfactory bulb, cerebellum and pons), and a consistent threshold was applied, followed by the 'Analyze particles' function (default parameters except for a size filter of 100–10,000 $µm^2$) to retrieve an estimated total cell number for the selected area. Additionally, we manually measured the overall area containing GFP^+ cell populations. Necropsy brains were evaluated using epifluorescence microscopy.

For improved illustrative presentation of representative images of in situ β-hexosaminidase determination, first brightness and contrast were adapted individually in RGB colour images to account for differences in overall background brightness. Colour-specific brightness and contrast changes were performed with constant parameters between images (as RGB composite). For quantification, tiled sagittal bright-field images of whole-brain sections were obtained. The area positive for β-hexosaminidase was determined in the red channel; the area of the whole brain was based on the blue channel. Thresholding was performed using setAutoThreshold ('Default no-reset').

For better presentation of representative images of human ES cell-derived transplanted cells at higher magnification, images were postprocessed with despeckle and an unsharp mask filter.

For histological quantification of PAS stain intensity, RGB colour images were used, and contrast and brightness were adjusted with constant parameters between images. A region of interest (ROI) was selected in the CA3 subfield of the hippocampus. Stain unmixing was performed with the ImageJ package Colour Deconvolution 2 (version 2.1) using the 'H PAS' vector[80,81]. Measurement of the ROI was then performed for 'Colour_2' (magenta; R, 0.175429; G, 0.972277; B, 0.154605) using the 32-bit absorbance output data.

General data analysis and statistics

Data analysis and visualization was performed using the R programming language (version 4.2.0; with RStudio environment 2022.02.2 Build 485). In addition to R base packages, the following packages were used: cowplot 1.1.2, dplyr 1.10.0, ggplot 2 3.4.0, ggpubr 0.5.0, ggrepel 0.9.2, patchwork 1.2.0, RColorBrewer 1.1-3, readxl 1.4.3, stringr 1.5.1, survival 3.5-7, survminer 0.4.9, tibble 3.2.1 and tidyr 1.2.1. Final figures were designed using Adobe Illustrator (version 29.6).

Statistical tests were chosen on the basis of the type and distribution of data and are specified in the figure legends. A level of significance of 5% was chosen. Box plot elements represent the median (centre line), first and third quartiles (lower and upper hinges), and lowest and highest values within 1.5 times the IQR from the hinge (whiskers).

Reporting summary

Further information on research design is available in the Nature Portfolio Reporting Summary linked to this article.

Data availability

The supporting data for all graphs are provided along with this publication. If additional information for replication of this study is required, it will be available from the corresponding author on reasonable request. Source data are provided with this paper.

Code availability

Computational and statistical analyses were performed using freely available software packages. If additional information for replication of this study is required, it will be available from the corresponding author on reasonable request.

60. Schaefer, B. C., Schaefer, M. L., Kappler, J. W., Marrack, P. & Kedl, R. M. Observation of antigen-dependent CD8$^+$ T-cell/dendritic cell interactions in vivo. *Cell. Immunol.* **214**, 110–122 (2001).
61. Dai, X.-M. et al. Targeted disruption of the mouse colony-stimulating factor 1 receptor gene results in osteopetrosis, mononuclear phagocyte deficiency, increased primitive progenitor cell frequencies, and reproductive defects. *Blood* **99**, 111–120 (2002).
62. Hamanaka, S. et al. Generation of transgenic mouse line expressing Kusabira Orange throughout body, including erythrocytes, by random segregation of provirus method. *Biochem. Biophys. Res. Commun.* **435**, 586–591 (2013).
63. Rathinam, C. et al. Efficient differentiation and function of human macrophages in humanized CSF-1 mice. *Blood* **118**, 3119–3128 (2011).
64. Wilkinson, A. C. et al. Long-term ex vivo haematopoietic-stem-cell expansion allows nonconditioned transplantation. *Nature* **571**, 117–121 (2019).
65. Wilkinson, A. C., Ishida, R., Nakauchi, H. & Yamazaki, S. Long-term ex vivo expansion of mouse hematopoietic stem cells. *Nat. Protoc.* **15**, 628–648 (2020).
66. Fattorelli, N. et al. Stem-cell-derived human microglia transplanted into mouse brain to study human disease. *Nat. Protoc.* **16**, 1013–1033 (2021).
67. Szot, G. L. et al. Tolerance induction and reversal of diabetes in mice transplanted with human embryonic stem cell-derived pancreatic endoderm. *Cell Stem Cell* **16**, 148–157 (2015).
68. Mayumi, H. & Good, R. A. Long-lasting skin allograft tolerance in adult mice induced across fully allogeneic (multimajor H-2 plus multiminor histocompatibility) antigen barriers by a tolerance-inducing method using cyclophosphamide. *J. Exp. Med.* **169**, 213–238 (1989).
69. Matsuura, A. et al. Cyclophosphamide-induced tolerance in fully allogeneic heart transplantation in mice. *Cell. Immunol.* **155**, 501–507 (1994).
70. Dodd-o, J. M. et al. Induction of major histocompatibility complex-mismatched mouse lung allograft acceptance with combined donor bone marrow: lung transplant using a 12-hour nonmyeloablative conditioning regimen. *Transplantation* **100**, e140 (2016).
71. Red blood cell lysis buffer. *Cold Spring Harb. Protoc.* https://doi.org/10.1101/pdb.rec390 (2006).
72. Guyenet, S. J. et al. A simple composite phenotype scoring system for evaluating mouse models of cerebellar ataxia. *J. Vis. Exp.* https://doi.org/10.3791/1787 (2010).
73. Ullman-Culleré, M. H. & Foltz, C. J. Body condition scoring: a rapid and accurate method for assessing health status in mice. *Lab. Anim. Sci.* **49**, 319–323 (1999).
74. Naserian, S. et al. Simple, reproducible, and efficient clinical grading system for murine models of acute graft-versus-host disease. *Front. Immunol.* **9**, 10 (2018).
75. Verlaat, L. et al. Novel pre-clinical mouse models for chronic graft-versus-host disease. *Front. Immunol.* **13**, 1079921 (2023).
76. Tribromoethanol (avertin). *Cold Spring Harb. Protoc.* https://doi.org/10.1101/pdb.rec701 (2006).
77. Skordos, I., Demeyer, A. & Beyaert, R. Analysis of T cells in mouse lymphoid tissue and blood with flow cytometry. *STAR Protoc.* **2**, 100351 (2021).
78. Challen, G. A., Boles, N., Lin, K.-Y. K. & Goodell, M. A. Mouse hematopoietic stem cell identification and analysis. *Cytometry A* **75A**, 14–24 (2009).
79. Bourgoin, C. et al. Widespread distribution of β-hexosaminidase activity in the brain of a Sandhoff mouse model after coinjection of adenoviral vector and mannitol. *Gene Ther.* **10**, 1841–1849 (2003).
80. Ruifrok, A. C. & Johnston, D. A. Quantification of histochemical staining by color deconvolution. *Anal. Quant. Cytol. Histol.* **23**, 291–299 (2001).
81. Landini, G., Martinelli, G. & Piccinini, F. Colour deconvolution: stain unmixing in histological imaging. *Bioinformatics* **37**, 1485–1487 (2021).

Acknowledgements We would like to thank all members of the Wernig laboratory, as well as A. Wilkinson, H. Nakauchi, M. Miyauchi and K. Niizuma, for helpful discussions throughout the project. We thank A. Lang and M. Vangipuram for administrative support, and we thank the FACS core at the Institute for Stem Cell Biology and Regenerative Medicine, especially C. Crumpton and C. Pan, and the Stanford Neuroscience Microscopy Service (supported by NIH NS069375) and G. Wang for technical support. We thank T. Südhof and Z. Liu for training and access to equipment for behavioural studies. We thank E. E. Graves for advice regarding small animal irradiation and calibration of the irradiation restrainer. *Csf1r*$^{-/-}$ (FVB.129×1-Csf1r^{tm1Ers}) mice were a gift from R. Stanley (Albert Einstein College of Medicine). B6.KUO mice were generated at the University of Tokyo and were a gift from H. Nakauchi. This work was supported by the Helen C. and Robert J. Kleberg Foundation and a DISC-0 award from the California Institute for Regenerative Medicine (DISC0-13875). M.M.-D.M. was supported by the German Research Foundation (Deutsche Forschungsgemeinschaft (DFG), MA 8492/1-1). Y.Y. was supported by the New York Stem Cell Foundation Druckenmiller Fellowship (NYSCF-D-F74). T.U. was supported by the Wu Tsai Neurosciences Institute Knight Initiative for Brain Resilience Scholar Award.

Author contributions Study concept and design: M.M.-D.M. and M.W. Animal experiments: M.M.-D.M., A.S. and A.T.C. Histological analyses: M.M.-D.M., A.S. and A.T.C. Cell culture: M.M.-D.M., Y.Y., A.S. and T.U. Flow cytometry experiments: M.M.-D.M. and A.S. Drafting and major editing of original manuscript: M.M.-D.M. and M.W. All authors reviewed, revised and approved the final version of the paper.

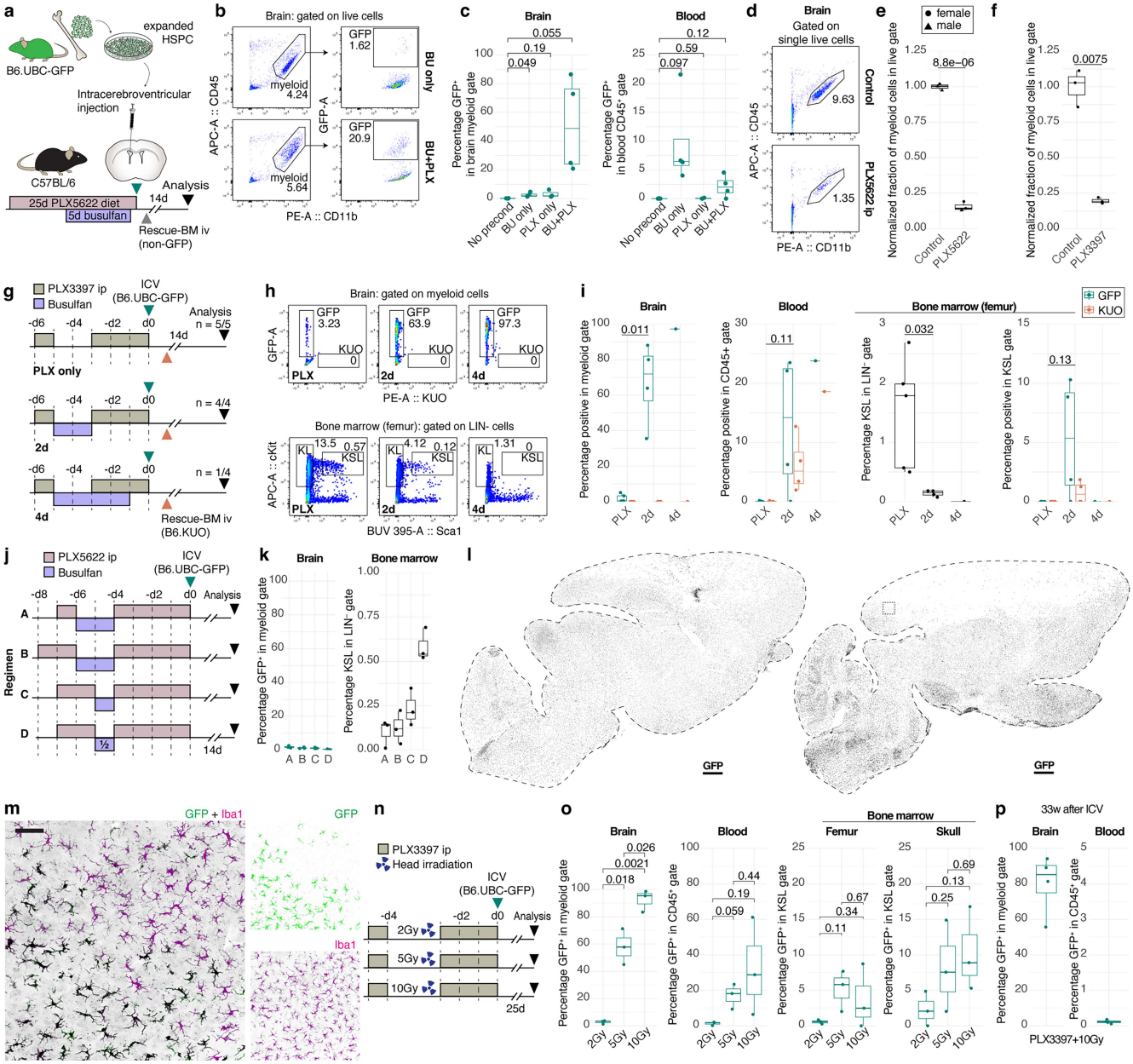
Competing interests M.W. is a co-founder of Neucyte, a scientific advisor for bit.bio, and co-founder and scientific advisor of Lytherian Therapeutics and Theseus Therapies. The other authors declare no competing interests. PLX5622 was provided by Plexxikon under a material transfer agreement between Stanford University and Plexxikon.

Additional information
Supplementary information The online version contains supplementary material available at https://doi.org/10.1038/s41586-025-09461-6.

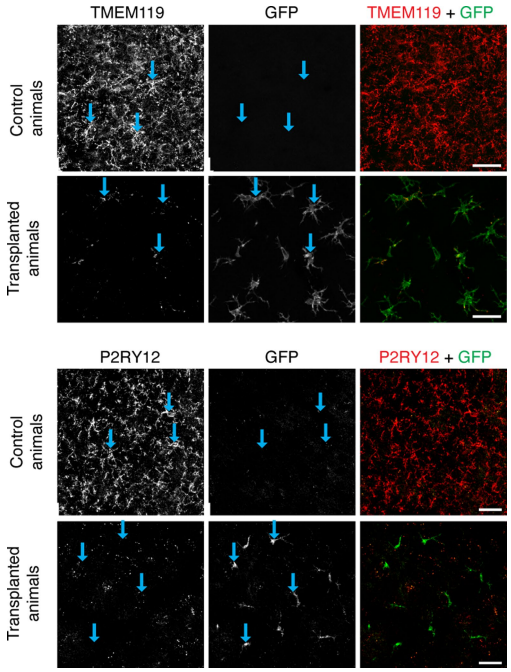
Correspondence and requests for materials should be addressed to Marius Wernig.

Peer review information *Nature* thanks the anonymous reviewers for their contribution to the peer review of this work.

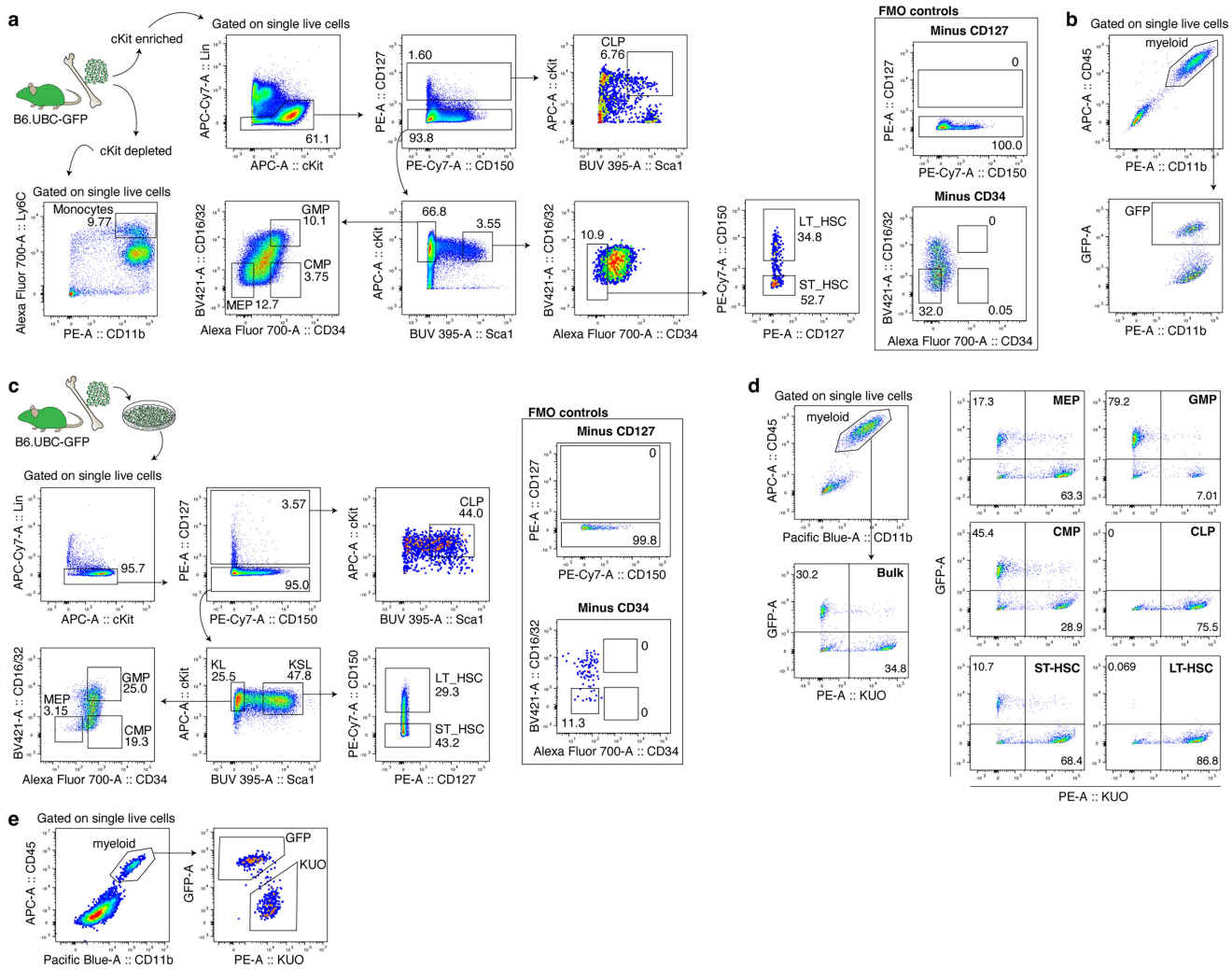
Reprints and permissions information is available at http://www.nature.com/reprints.



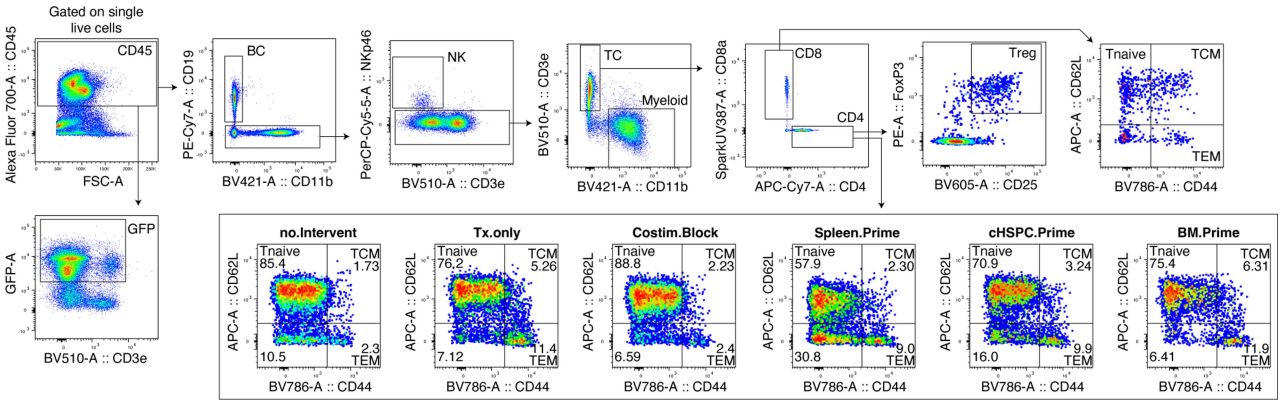
Extended Data Fig. 1 | Additional evaluation of the effects of CSF1R inhibitors and irradiation dose. a, Experimental design. The last injection of busulfan was applied one day before transplantation, and PLX5622 diet was withdrawn on the day of transplantation. 200 ×10^3 B6.UBC-GFP graft cells were transplanted per recipient animal. iv, intravenous. **b**, Representative flow cytometry plots and gating strategy. **c**, Quantification of donor derived GFP$^+$ chimerism in the peripheral blood and myeloid compartment of the contralateral brain hemisphere based on flow cytometry. n = 4, 4, 3, and 4 animals per group, respectively (from left to right). Two-sided Welch t-test. **d**, Evaluation of microglia depletion. Representative flow cytometry plots and gating strategy are shown for two female animals. **e**, Flow cytometric quantification. The brain was analyzed one day after the last PLX5622 injection. The drug was administered daily over 4 days. n = 3 animals per group. Two-sided Welch t-test. **f**, Flow cytometric quantification. The brain was analyzed one day after the last PLX3397 injection. The drug was administered daily over 3 days. n = 3 animals per group. Two-sided Welch t-test. **g**, Experimental design. 200 ×10^3 B6.UBC-GFP HSPC were transplanted per recipient animal. Numbers (n) represent assigned and survived animals per group. ip, intraperitoneal. **h**, Representative flow cytometry plots and gating strategy per experimental group. **i**, Flow cytometric quantification (contralateral brain hemisphere). n = 5, 4, and 1 animals per group, respectively (from left to right). Two-sided Welch t-test. **j**, Experimental outline. 200 ×10^3 B6.UBC-GFP HSPC were transplanted per recipient animal. n = 3 animals per group. **k**, Flow cytometric quantification (contralateral brain hemisphere). **l**, Immunofluorescent staining for GFP of sagittal brain sections of the ipsilateral hemisphere of two animals with irradiation+PLX3397 treatment. Shown are cortical areas of reduced donor cell engraftment density. Purple square illustrates magnified area of panel m. Scale bar = 200 µm. **m**, Immunofluorescent stain shows repopulated endogenous GFP$^-$ microglia and grafted GFP$^+$ cells. Demonstrated is the border between high-density donor cell repopulated brain and an area with low chimerism. Scale bar = 50 µm. **n**, Experimental outline. 200 ×10^3 B6.UBC-GFP HSPC were transplanted per recipient animal. n = 3 animals per group. **o**, Flow cytometric quantification (contralateral brain hemisphere). Two-sided Welch t-test. **p**, Flow cytometric quantification of myeloid donor chimerism in the brain and blood 33 weeks after ICV transplantation and preconditioning with PLX3397 and 10 Gy head irradiation. n = 4 animals. Box-plot elements in Extended Data Fig. 1 represent median (center line), first and third quartiles (lower and upper hinges) and smallest/highest value with at most 1.5*IQR (inter-quartile range) from the hinge (whiskers).



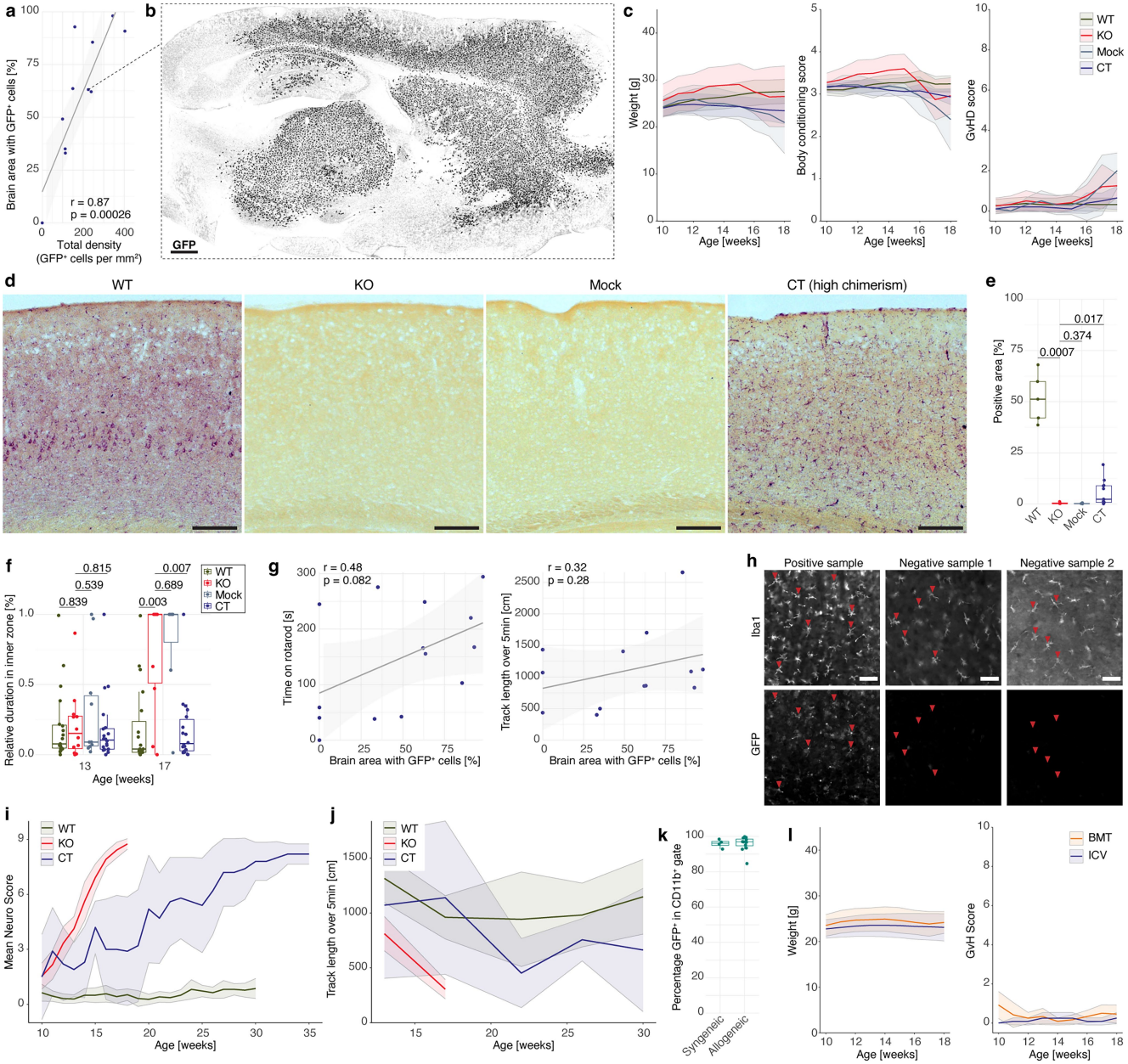
Extended Data Fig. 2 | Expression of microglial homeostatic marker proteins on transplanted myeloid cells. Representative immunofluorescent stain shows the expression of IBA1, P2RY12, and TMEM119 in endogenous GFP$^-$ microglia and grafted GFP$^+$ cells in the cortex. Grafted cells were evaluated 25 days after transplantation. Samples of three different animals per group were examined with comparable results. Scale bar = 30 µm.



Extended Data Fig. 3 | Flow cytometric gating strategies for hematopoietic stem and progenitor cells. Flow cytometry plots and gating strategies are provided for the sorting of primary bone marrow cells (**a**) and ex vivo expanded HSPCs (**c**), as well as for the quantification of GFP$^+$ or KUO$^+$ fractions in myeloid cells in vitro (**b**, **d**, **e**). FMO, fluorescence minus one.



Extended Data Fig. 4 | Flow cytometric gating strategy for peripheral blood evaluation. Flow cytometry plots and gating strategy for the evaluation of peripheral blood cells in the context of graft rejection. BC, B cells; NK, natural killer cells; TC, T cells; TCM, central memory T cells; TEM, effector memory T cells; Tnaive, naïve T cells; Treg, regulatory T cells.



Extended Data Fig. 5 | See next page for caption.

Extended Data Fig. 5 | Additional characterization of allogeneic microglia replacement as a cell therapy. a, Engraftment of GFP$^+$ donor cells in the cerebrum ~12 weeks after transplantation. Shown as total density and relative engrafted brain area. n = 12 CT animals. Regression line based on linear model (shaded area = confidence interval); r = Pearson correlation coefficient. Two-sided test. **b**, Representative GFP immunofluorescence image of a sagittal brain section. Dotted line indicates replicate in panel a. Scale bar = 500 µm. **c**, Body weight and conditioning score as well as GvHD score demonstrated for live animals of the experimental groups. A late increase in GvHD score especially in the KO and Mock groups coincided with neurological decline and was primarily based on weight loss and hunching. No occurrences of skin fibrosis or diarrhea were detected in this cohort. Lines represent the mean with 95% confidence interval. n = 61 animals total (WT = 19, KO = 12, Mock = 10, CT = 20). **d**, Representative images of in situ β-hexosaminidase determination in the cortex. A total of 27 animals were evaluated. Scale bar = 200 µm. **e**, Quantification of the β-hexosaminidase positive area in the whole brain. A total of 27 animals were evaluated. Two-sided Welch t-test. **f**, Quantification of relative time spent in the inner zone of an open field setup over 5 min. Deceased animals were excluded from the analysis. n = 19, 12, 10, and 20 animals (13 weeks) and 19, 10, 7, and 18 animals (17 weeks) in the WT, KO, Mock, and CT group, respectively. Two-sided Mann–Whitney U test. **g**, Correlation between brain area of engrafted cells and clinical variables. In two animals with mortality before week 18, engraftment was evaluated in necropsy tissue, and no GFP$^+$ cells were detected (see panel h). n = 14 CT animals. Regression line based on linear model (shaded area = confidence interval); r = Pearson correlation coefficient. Two-sided test. **h**, Immunofluorescent images of necropsy brain tissue. Positive sample represents a CT animal with unclear mortality on day 114. Negative samples 1 and 2 represent CT animals with mortality due to neurological decline before 18 weeks of age, and no detected GFP$^+$ myeloid cells in the brain. Red arrows illustrate present or absent colocalization of Iba1 and GFP. Scale bar = 50 µm. **i**, Neuro Score displayed for WT (n = 19 animals up to week 18, then 11 animals), KO (n = 12), and long-term CT (n = 5) animals. Deceased animals received a maximum score of 9. Lines represent the mean with 95% confidence interval. **j**, Quantification of locomotor activity in an open field setup over 5 min (performed at 13, 17, 22, 26, and 30 weeks of age). Displayed for WT (n = 19 animals up to week 17, then 11 animals), KO (n = 10 and 12 animals at weeks 17 and 13, respectively) and long-term CT (n = 5 animals up to week 17, then 4 animals) animals. Deceased animals were excluded from the analysis. Lines represent the mean with 95% confidence interval. **k**, Flow cytometric quantification of myeloid donor chimerism in the peripheral blood after bone marrow transplantation (BMT). syngeneic control n = 4 animals (6 weeks after BMT). allogeneic with co-stimulation blockade n = 12 animals (7×6 weeks and 5×12 weeks after BMT). **l**, Body weight and GvHD score. Lines represent the mean with 95% confidence interval. n = 12 animals per group. Box-plot elements in Extended Data Fig. 5 represent median (center line), first and third quartiles (lower and upper hinges) and smallest/highest value with at most 1.5*IQR (inter-quartile range) from the hinge (whiskers).

Extended Data Table 1 | Scores used for behavioral assessment

Neuro Score

Criteria	0	0.5	1	2	3
Hindlimb clasping	Both hindlimbs are splayed outwards for >50% of test period	One hindlimb is partially retracted towards abdomen for >50% of test period	One hindlimb is fully retracted against abdomen for >50% of test period	Both hindlimbs are partially retracted towards abdomen for >50% of test period	Both hindlimbs are fully retracted and touching the abdomen for >50% of test period
Gait	No tremor or limp present, gait is normal and mouse is freely mobile	Mild tremor present while walking	Moderate tremor or limp present while walking	Severe tremor or limp, lowered pelvis while walking, diminished walking ability but still mobile	Extreme difficulty in progressing forward, immobile
Ledge	Mouse walks along ledge without losing balance, uses hindlimbs to lower self into cage without difficulty	Mouse slips on ledge but descends into cage properly	Mouse's landing is slightly modified (small hop to ground, face touches ground) but mouse is otherwise coordinated	Mouse lands on head instead of paws when descending into cage	Mouse fails to use hindlimbs to lower self into cage, falls off ledge completely, or refuses to move despite gentle nudging

Graft-versus-host disease (GvHD) Score

Criteria	0	1	2
Weight loss	<10% of previous body weight	>10% of previous body weight	>25% of previous body weight
Hunched posture	Normal posture	Hunched posture present while resting	Hunched posture persists when walking
Alopecia	Not present	<2cm hair loss	>2cm hair loss
Skin fibrosis	Not present	Small patches of red, hard, or thickened skin	Significant skin lesions present
Diarrhea	Not present	Mild diarrhea	Persistent or severe diarrhea

nature portfolio

Corresponding author(s): Marius Wernig

Last updated by author(s): Jul 13, 2025

Reporting Summary

Nature Portfolio wishes to improve the reproducibility of the work that we publish. This form provides structure for consistency and transparency in reporting. For further information on Nature Portfolio policies, see our Editorial Policies and the Editorial Policy Checklist.

Statistics

For all statistical analyses, confirm that the following items are present in the figure legend, table legend, main text, or Methods section.

n/a	Confirmed	
☐	☒	The exact sample size (*n*) for each experimental group/condition, given as a discrete number and unit of measurement
☐	☒	A statement on whether measurements were taken from distinct samples or whether the same sample was measured repeatedly
☐	☒	The statistical test(s) used AND whether they are one- or two-sided *Only common tests should be described solely by name; describe more complex techniques in the Methods section.*
☒	☐	A description of all covariates tested
☒	☐	A description of any assumptions or corrections, such as tests of normality and adjustment for multiple comparisons
☐	☒	A full description of the statistical parameters including central tendency (e.g. means) or other basic estimates (e.g. regression coefficient) AND variation (e.g. standard deviation) or associated estimates of uncertainty (e.g. confidence intervals)
☐	☒	For null hypothesis testing, the test statistic (e.g. *F*, *t*, *r*) with confidence intervals, effect sizes, degrees of freedom and *P* value noted *Give P values as exact values whenever suitable.*
☒	☐	For Bayesian analysis, information on the choice of priors and Markov chain Monte Carlo settings
☒	☐	For hierarchical and complex designs, identification of the appropriate level for tests and full reporting of outcomes
☐	☒	Estimates of effect sizes (e.g. Cohen's *d*, Pearson's *r*), indicating how they were calculated

Our web collection on statistics for biologists contains articles on many of the points above.

Software and code

Policy information about availability of computer code

Data collection	ZEN blue (Zeiss, version 3.7.97.04000 and version 3.8.99.03000) Leica Application Suite X (Leica, 3.7.1.21655) BIOBSERVE Viewer3 software (version 3.0.1.442)
Data analysis	Fiji/ImageJ (NIH, version 1.54f) ImageJ package Colour Deconvolution 2 (version 2.1) FlowJo software (version 10.8.1) Adobe Illustrator (version 29.6; for design of final figures) R programming language (version 4.2.0; with RStudio environment 2022.02.2 Build 485) and R base packages Additional R packages: cowplot 1.1.2, dplyr 1.10.0, ggplot 2 3.4.0, ggpubr 0.5.0, ggrepel 0.9.2, patchwork 1.2.0, RColorBrewer 1.1-3, readxl 1.4.3, stringr 1.5.1, survival 3.5-7, survminer 0.4.9, tibble 3.2.1, tidyr 1.2.1

For manuscripts utilizing custom algorithms or software that are central to the research but not yet described in published literature, software must be made available to editors and reviewers. We strongly encourage code deposition in a community repository (e.g. GitHub). See the Nature Portfolio guidelines for submitting code & software for further information.

Data

Policy information about availability of data

All manuscripts must include a data availability statement. This statement should provide the following information, where applicable:

- Accession codes, unique identifiers, or web links for publicly available datasets
- A description of any restrictions on data availability
- For clinical datasets or third party data, please ensure that the statement adheres to our policy

The source data of all graphs is provided along with this publication. If additional information for replication of this study is required, it will be available from the corresponding author upon reasonable request.

Research involving human participants, their data, or biological material

Policy information about studies with human participants or human data. See also policy information about sex, gender (identity/presentation), and sexual orientation and race, ethnicity and racism.

Reporting on sex and gender	not applicable
Reporting on race, ethnicity, or other socially relevant groupings	not applicable
Population characteristics	not applicable
Recruitment	not applicable
Ethics oversight	not applicable

Note that full information on the approval of the study protocol must also be provided in the manuscript.

Field-specific reporting

Please select the one below that is the best fit for your research. If you are not sure, read the appropriate sections before making your selection.

☒ Life sciences ☐ Behavioural & social sciences ☐ Ecological, evolutionary & environmental sciences

For a reference copy of the document with all sections, see nature.com/documents/nr-reporting-summary-flat.pdf

Life sciences study design

All studies must disclose on these points even when the disclosure is negative.

Sample size	No sample size calculation was performed due to the novel biology underlying the experiments. Where possible, samples size estimation was based on existing literature and/or empirical knowledge (e.g. Shibuya et al. 2022, Yoo et al. 2023, Mader et al. 2024, Norflus et al. 1998).
Data exclusions	Data exclusions were indicated in the manuscript and/or figures/figure legends. This concerned one animal with unclear early mortality that appeared unrelated to the studied outcome in the HexB CT group. Moreover, animals with periprocedural mortality (up to 2 weeks after transplantation) were excluded from the analysis of this cohort.
Replication	The replicates of the experiments are indicated in figures / figure legends.
Randomization	For experiments involving animals: Animals were randomly assigned to experimental groups (controlling for equal sex ratios where applicable). Tissue samples for specific analyses were randomly selected (if not all samples were processed). For cell culture experiments: Donor cells were plated into wells with cultured primary glia based on random selection of plates and wells.
Blinding	Blinding was performed for the behavioral assessment and survival analysis of HexB knockout animals. While this was limited due to surgical wounds in certain experimental groups, the behavioral investigator was blinded for the injected cells (CT vs Mock). For animals with flow cytometric or histological readout, animal IDs without indication of the experimental group were used for sample processing.

Reporting for specific materials, systems and methods

We require information from authors about some types of materials, experimental systems and methods used in many studies. Here, indicate whether each material, system or method listed is relevant to your study. If you are not sure if a list item applies to your research, read the appropriate section before selecting a response.

Materials & experimental systems

n/a	Involved in the study
☐	☒ Antibodies
☐	☒ Eukaryotic cell lines
☒	☐ Palaeontology and archaeology
☐	☒ Animals and other organisms
☒	☐ Clinical data
☒	☐ Dual use research of concern
☒	☐ Plants

Methods

n/a	Involved in the study
☒	☐ ChIP-seq
☐	☒ Flow cytometry
☒	☐ MRI-based neuroimaging

Antibodies

Antibodies used

Immunoflurescence
anti-GFP (abcam, ab13970)
anti-Iba1 (FUJIFILM Wako, 019-19741)
anti-P2RY12 (Sigma, HPA014518)
anti-P2RY12 (Biolegend, 848002)
anti-TMEM119 (Invitrogen, PA5-62505)
anti-TMEM119 (abcam, ab209064)

Flow cytometry
CD3e (clone 145-2C11, Biolegend 100308 / 100353, 1:200), CD4 (clone GK1.5, Biolegend 100414, 1:200), CD8a (clone 53-6.7, Biolegend 100798, 1:200), CD11b (clone M1/70, Biolegend 101208 / 101224 / 101236, 1:200), CD16/32 (clone 93, Biolegend 101331, 1:300), CD19 (clone 6D5, Biolegend 115520, 1:200), CD25 (clone PC61, Biolegend 102036, 1:100), CD34 (clone RAM34, BD 560518, 1:100), CD44 (clone IM7, Biolegend 103059, 1:200), CD45 (clone 2D1, Biolegend 368512, 1:20), CD45 (clone 30-F11, Biolegend 103112 / 103128, 1:200), CD48 (clone HM48-1, Biolegend 103428, 1:300), CD62L (clone MEL-14, Biolegend 104411, 1:200), CD127 (clone SB/199, Biolegend 121112, 1:300), CD150 (clone TC15-12F12.2, Biolegend 115913, 1:300), FoxP3 (clone 150D, Biolegend 320008, 1:50), cKit (clone 2B8, Invitrogen 17-1171-83, 1:300), Ly6c (clone HK1.4, Biolegend 128023, 1:300), NKp46 (clone 29A1.4, Biolegend 137609, 1:100), Sca1 (clone D7, Biolegend 108108 or BD 563990, 1:300), Streptavidin (BD, 554063, 1:300), Lineage biotin-antibody cocktail (Miltenyi Biotec, 130-090-858, 1:100)

In vivo antibody treatment
InVivoMAb anti-mouse CD40L (CD154; Bio X Cell)
InVivoMAb recombinant CTLA-4-Ig (hum/hum; Bio X Cell)

Validation

All antibodies used in this study are commercially available and have been used in previous studies and/or validated as indicated on the manufacturer's website. Specifically:

anti-GFP (abcam, ab13970)
https://www.abcam.com/en-us/products/primary-antibodies/gfp-antibody-ab13970
Suitable for: WB, ICC/IF; Reacts with: Species independent
3612 associated publications on manufacturer website

anti-Iba1 (FUJIFILM Wako, 019-19741)
https://labchem-wako.fujifilm.com/us/product/detail/W01W0101-1974.html
Reactivity : mouse, rat; Applications Immunohistochemistry (Frozen Section)
5196 citations on manufacturer website

anti-P2RY12 (Sigma, HPA014518)
https://www.sigmaaldrich.com/US/en/product/sigma/hpa014518
Reacts with: human; immunohistochemistry validation stain shown on website

anti-P2RY12 (Biolegend, 848002)
https://www.biolegend.com/en-us/products/purified-anti-mouse-p2ry12-antibody-14063
Verified Reactivity: Mouse; immunohistochemistry validation stain shown on website
21 product citations

anti-TMEM119 (Invitrogen, PA5-62505)
https://www.thermofisher.com/antibody/product/TMEM119-Antibody-Polyclonal/PA5-62505
Species Reactivity: Human; immunohistochemistry validation stain shown on website

anti-TMEM119 (abcam, ab209064)
https://www.abcam.com/en-us/products/primary-antibodies/tmem119-antibody-28-3-microglial-marker-ab209064?
Tested reactivity: Mouse; immunofluorescence validation stain shown on website
139 product citations

anti-CD3e (clone 145-2C11)
See e.g. Skordos et al. 2021 (doi: 10.1016/j.xpro.2021.100351)
https://www.biolegend.com/en-us/products/pe-anti-mouse-cd3epsilon-antibody-25

Verified Reactivity Mouse, Application flow cytometry - Quality tested

anti-CD4 (clone GK1.5)
See e.g. Skordos et al. 2021 (doi: 10.1016/j.xpro.2021.100351)
https://www.biolegend.com/en-us/products/apc-cyanine7-anti-mouse-cd4-antibody-1964
Verified Reactivity Mouse, Application flow cytometry - Quality tested

anti-CD8a (clone 53-6.7)
See e.g. Skordos et al. 2021 (doi: 10.1016/j.xpro.2021.100351)
https://www.biolegend.com/en-us/products/spark-uv-387-anti-mouse-cd8a-antibody-22117
Verified Reactivity Mouse, Application flow cytometry - Quality tested

anti-CD11b (clone M1/70)
https://www.biolegend.com/en-us/products/pe-anti-mouse-human-cd11b-antibody-349
Verified Reactivity Mouse, Human, Cynomolgus, Rhesus, Application flow cytometry - Quality tested

anti-CD16/32 (clone 93)
https://www.biolegend.com/en-us/products/brilliant-violet-421-anti-mouse-cd16-32-antibody-8598
Verified Reactivity Mouse, Application flow cytometry - Quality tested

anti-CD19 (clone 6D5)
https://www.biolegend.com/en-us/products/pe-cyanine7-anti-mouse-cd19-antibody-1907
Verified Reactivity Mouse, Application flow cytometry - Quality tested

anti-CD25 (clone PC61)
See e.g. Skordos et al. 2021 (doi: 10.1016/j.xpro.2021.100351)
https://www.biolegend.com/en-us/products/brilliant-violet-605-anti-mouse-cd25-antibody-7639
Verified Reactivity Mouse, Application flow cytometry - Quality tested

anti-CD34 (clone RAM34)
See e.g. Wilkinson et al. 2020 (doi: 10.1038/s41596-019-0263-2)
https://www.bdbiosciences.com/en-us/products/reagents/flow-cytometry-reagents/research-reagents/single-color-antibodies-ruo/alexa-fluor-700-rat-anti-mouse-cd34.560518
Reactivity: Mouse (QC Testing)
Application: Flow cytometry (Routinely Tested)

anti-CD44 (clone IM7)
See e.g. Skordos et al. 2021 (doi: 10.1016/j.xpro.2021.100351)
https://www.biolegend.com/en-us/products/brilliant-violet-785-anti-mouse-human-cd44-antibody-7959
Verified Reactivity Mouse Human, Application flow cytometry - Quality tested

anti-CD45 (clone 2D1)
https://www.biolegend.com/en-us/products/apc-anti-human-cd45-antibody-12397
Verified Reactivity Human, Application flow cytometry - Quality tested

anti-CD45 (clone 30-F11)
https://www.biolegend.com/en-us/products/apc-anti-mouse-cd45-antibody-97
Verified Reactivity Mouse, Application flow cytometry - Quality tested

anti-CD48 (clone HM48-1)
https://www.biolegend.com/en-us/products/brilliant-violet-421-anti-mouse-cd48-antibody-7327
Verified Reactivity Mouse, Application flow cytometry - Quality tested

anti-CD62L (clone MEL-14)
See e.g. Skordos et al. 2021 (doi: 10.1016/j.xpro.2021.100351)
https://www.biolegend.com/en-us/products/apc-anti-mouse-cd62l-antibody-381
Verified Reactivity Mouse, Application flow cytometry - Quality tested

anti-CD127 (clone SB/199)
https://www.biolegend.com/en-us/products/pe-anti-mouse-cd127-il-7ralpha-antibody-3265
Verified Reactivity Mouse, Application flow cytometry - Quality tested

anti-CD150 (clone TC15-12F12.2)
See e.g. Wilkinson et al. 2020 (doi: 10.1038/s41596-019-0263-2)
https://www.biolegend.com/en-us/products/pe-cyanine7-anti-mouse-cd150-slam-antibody-3056
Verified Reactivity Mouse, Application flow cytometry - Quality tested

anti-FoxP3 (clone 150D)
https://www.biolegend.com/en-us/products/pe-anti-mouse-rat-human-foxp3-antibody-2889
Verified Reactivity Human, Mouse, Rat, Application intracellular flow cytometry - Quality tested

anti-cKit (clone 2B8)
See e.g. Wilkinson et al. 2020 (doi: 10.1038/s41596-019-0263-2)
https://www.thermofisher.com/antibody/product/CD117-c-Kit-Monoclonal-Antibody-2B8-APC-eBioscience/17-1171-83
Species Reactivity: Mouse, Pig;
Applications Reported: The 2B8 antibody has been reported for use in flow cytometric analysis.

Applications Tested: The 2B8 antibody has been tested by flow cytometric analysis of mouse bone marrow cells.

anti-Ly6c (clone HK1.4)
https://www.biolegend.com/en-us/products/alexa-fluor-700-anti-mouse-ly-6c-antibody-6757
Verified Reactivity Mouse, Application flow cytometry - Quality tested

anti-NKp46 (clone 29A1.4)
https://www.biolegend.com/en-us/products/percp-cyanine5-5-anti-mouse-cd335-nkp46-antibody-6724
Verified Reactivity Mouse, Application flow cytometry - Quality tested

anti-Sca1 (clone D7)
See e.g. Wilkinson et al. 2020 (doi: 10.1038/s41596-019-0263-2)
https://www.biolegend.com/en-us/products/pe-anti-mouse-ly-6a-e-sca-1-antibody-228
Verified Reactivity Mouse, Application flow cytometry - Quality tested
https://www.bdbiosciences.com/en-us/products/reagents/flow-cytometry-reagents/research-reagents/single-color-antibodies-ruo/buv395-rat-anti-mouse-ly-6a-e.563990
Reactivity: Mouse (QC Testing)
Application: Flow cytometry (Routinely Tested)

anti-Streptavidin (BD, 554063, 1:300)
https://www.bdbiosciences.com/en-us/products/reagents/flow-cytometry-reagents/research-reagents/single-color-antibodies-ruo/streptavidin-apc-cy-7.554063
Application: Flow cytometry (Routinely Tested)

Lineage biotin-antibody cocktail (Miltenyi Biotec, 130-090-858, 1:100)
See e.g. Shibuya et al. 2022 (doi: 10.1126/scitranslmed.abl9945)
Application: flow cytometry of mouse bone marrow

Eukaryotic cell lines

Policy information about cell lines and Sex and Gender in Research

Cell line source(s)	H1 (WA01), human embryonic stem cell, male, purchased from WiCell
Authentication	The cell line was monitored for morphological and growth properties.
Mycoplasma contamination	The cell line was regularly tested for mycoplasma contamination
Commonly misidentified lines (See ICLAC register)	no commonly misidentified lines were used

Animals and other research organisms

Policy information about studies involving animals; ARRIVE guidelines recommended for reporting animal research, and Sex and Gender in Research

Laboratory animals	Experimental animals were 6-13 weeks old at the timepoint of cell transplantation, unless otherwise specified in the manuscript. The following strains were used: C57BL/6J (JAX, Strain 00066) FVB/NJ (JAX, Strain 001800) C57BL/6-Tg(UBC- GFP)30Scha/J strain (JAX, Strain 004353) CSF1R-KO mice (FVB.129X1-Csf1rtm1Ers); gift from Dr. Richard Stanley, Albert Einstein College of Medicine, New York, USA) KUO mice (C57BL/6 background) express the fluorescent protein Kusabira Orange in the hematopoietic lineage (Hamanaka, S. et al. Generation of transgenic mouse line expressing Kusabira Orange throughout body, including erythrocytes, by random segregation of provirus method. Biochemical and Biophysical Research Communications 435, 586–591 (2013)) C;129S4-Rag2tm1.1Flv Csf1tm1(CSF1)Flv Il2rgtm1.1Flv/J (JAX, Strain 017708) B6;129S-Hexb<tm1Rlp>/J (JAX, Strain 002914)
Wild animals	no wild animals were used for this study
Reporting on sex	Sex of experimental animals is indicated in the methods, figures, and/or figure legends.
Field-collected samples	no field collected samples were used
Ethics oversight	All animal procedures were approved by the administrative panel on laboratory animal care at Stanford University (APLAC21565).

Note that full information on the approval of the study protocol must also be provided in the manuscript.

Plants

Seed stocks	na
Novel plant genotypes	na
Authentication	na

Flow Cytometry

Plots

Confirm that:

☒ The axis labels state the marker and fluorochrome used (e.g. CD4-FITC).

☒ The axis scales are clearly visible. Include numbers along axes only for bottom left plot of group (a 'group' is an analysis of identical markers).

☒ All plots are contour plots with outliers or pseudocolor plots.

☒ A numerical value for number of cells or percentage (with statistics) is provided.

Methodology

Sample preparation	Brains were first minced with a razorblade, and then transferred into ice-cold HBSS without Ca2+/Mg2+ (Gibco). The tissue was then enzymatically dissociated using the Neural Tissue Dissociation Kit P (Miltenyi Biotec) in accordance with the manufacturer's protocol. The total incubation time at 37°C was 35min, afterwards the tissue was kept on ice or at 4°C. After washing with ice-cold HBSS (with Ca2+/Mg2+) and running through a 70µm cell strainer, a gradient centrifugation was performed using a 30% Percoll/HBSS solution (Cytiva Percoll™ Centrifugation Media) at 700G for 10min. After washing the resulting cell pellet with PBS, it was resuspended in Flow buffer (PBS with 5% cosmic calf serum) with antibodies for 20min at 4°C. Peripheral blood was first incubated for 10 minutes in ice-cold RBC lysis buffer. After washing in PBS, cells were resuspended in Flow buffer with antibodies. Samples were incubated for 15-30min at 4°C depending on the panel. The evaluation of peripheral blood immune cells including lymphocyte populations was adapted from Skordos et al. using the following staining workflow: First, a dead/live stain was performed using Zombie Red™ (Biolegend, 423109), cells were then incubated with anti-mouse CD16/CD32 (Mouse BD Fc Block™, BD, 553141), and then a surface antigen stain was performed as described above. Cells were then fixed, permeabilized, and intracellularly stained (True-Nuclear™ Transcription Factor Buffer Set). Bone marrow cells were extracted, optionally incubated in RBC lysis buffer. For sorting of HSPC, cells were additionally enriched for cKit expression via MACS as detailed in the manuscript. For staining, first, samples were incubated with an antibody mix for lineage marker for 30min at room temperature (Miltenyi Biotec, 130-090-858). Then, staining for other antibodies was performed with incubation times of 30-90min depending on the panel used. In vitro samples were dissociated via incubation with trypsin for 5min at 37°C, then quenched with Flow buffer, and spun down. The cell pellet was then resuspended in Flow buffer with antibodies and incubated for 15min at 4°C. For all samples, after completion of the stain incubation time, samples were washed with PBS, and pellets then resuspended in Flow buffer with dead/live stain for non-fixed samples, and kept on ice for analysis.
Instrument	Flow cytometry was performed on a BD FACS Aria II or a BD CytoFLEX.
Software	FACSDiva and CytExpert (BD Biosciences), FlowJo (version 10.8.1)
Cell population abundance	A regular monitoring of post-sort cell abundance was not feasible for experiments in this study, due to the generally small number of cells sorted directly into cell culture dishes for in vitro cultivation. All experiments were performed on cytometers in the FACS Core at the Stanford Institute for Stem Cell Biology and Regenerative Medicine, which are regularly maintenanced and monitored by the FACS core staff.
Gating strategy	The gating strategies for the different experiments are exemplified in the figures and extended data figures.

☒ Tick this box to confirm that a figure exemplifying the gating strategy is provided in the Supplementary Information.